
Estimating the limiting shape of bivariate scaled sample clouds for self-consistent inference of extremal dependence properties

Emma S. Simpson^{1*} and Jonathan A. Tawn²

¹Department of Statistical Science, University College London, Gower Street, London, WC1E 6BT, U.K.

²Department of Mathematics and Statistics, Lancaster University, LA1 4YF, U.K.

July 7, 2022

Abstract

An integral part of carrying out statistical analysis for bivariate extreme events is characterising the tail dependence relationship between the two variables. For instance, we may be interested in identifying the presence of asymptotic dependence and/or in determining whether an individual variable can be large while the other is of smaller order. In the extreme value theory literature, various techniques are available to assess or model different aspects of tail dependence; currently, inference must be carried out separately for each of these, with the possibility of contradictory conclusions. Recent developments by [Nolde and Wadsworth \(2022\)](#) have established theoretical links between different characterisations of extremal dependence, through studying the limiting shape of an appropriately-scaled sample cloud. We exploit these results for inferential purposes, by first developing an estimator for the sample limit set and then using this to deduce self-consistent estimates for the extremal dependence properties of interest. In simulations, the limit set estimates are shown to be successful across a range of distributions, and the estimates of dependence features are individually competitive with existing estimation techniques, and jointly provide a major improvement. We apply the approach to a data set of sea wave heights at pairs of locations, where the estimates successfully capture changes in the limiting shape of the sample cloud as the distance between the locations increases, including the weakening extremal dependence that is expected in environmental applications.

Keywords: bivariate extremes; coefficient of asymptotic independence; conditional extremes; extremal dependence structure; gauge function; sample cloud

Acknowledgements This publication is based upon work supported by the King Abdullah University of Science and Technology (KAUST) Office of Sponsored Research (OSR) under Award No. OSR-2017-CRG6-3434.02. We thank Philip Jonathan and Jennifer Wadsworth for providing access to the data studied in Section [5.3](#).

*Corresponding author. Email address: emma.simpson@ucl.ac.uk

1 Introduction

In the statistical analysis of bivariate extreme events, tail dependence features are a key consideration. It is common to categorise pairs of variables as being *asymptotically dependent*, when the most extreme values can occur simultaneously in both variables, or *asymptotically independent*, when they cannot (Coles et al., 1999). Specifically when the variables X_1 and X_2 follow an identical marginal distribution whose support has an infinite upper endpoint, as will be the case later in this paper, this can be formalised through the extremal dependence measure

$$\chi = \lim_{x \rightarrow \infty} \Pr(X_2 > x \mid X_1 > x). \quad (1)$$

Having $\chi > 0$ coincides with asymptotic dependence between X_1 and X_2 , while $\chi = 0$ under the asymptotic independence setting. Since many models for bivariate extremes are only suitable in one of these situations, distinguishing between them can play a crucial role in model selection. Further, in the case of asymptotic dependence, in addition to both variables taking their largest values simultaneously, it is possible that at least one of them could be large while the other is small, i.e., the variables may have a more complicated extremal dependence structure; see Goix et al. (2017) or Simpson et al. (2020), for example. In such cases, models that are able to capture a mixture structure in the extremal dependence features are required, with Tendijck et al. (2022) giving a first approach to this.

In the extreme value theory literature, various methods are available to assess or model these tail dependence features, and to quantify levels of extremal dependence. In Section 2.2, we introduce the approaches we focus on, with associated measures that describe the extremal dependence setting. Existing methods carry out inference separately for each of these extremal dependence measures, with no guarantee of obtaining self-consistent information about the tail dependence behaviour across the different ones. For instance, estimates of some measures could indicate asymptotic dependence between variables, while others show asymptotic independence, thus leading to the possibility of unhelpful contradictions.

Recent developments by Nolde and Wadsworth (2022) have established theoretical links between different characterisations of extremal dependence. For a given joint distribution, their results allow for the calculation of various extremal dependence measures, by considering the limiting shape of the sample cloud, under suitable scaling. This approach was motivated by results from Nolde (2014), who first showed how to calculate the coefficient of asymptotic independence of Ledford and Tawn (1996) in a similar way.

We develop a first approach to estimate the asymptotic, scaled sample cloud boundary. We then aim to exploit this, along with the theoretical results of Nolde (2014) and Nolde and Wadsworth (2022), to obtain estimates of several bivariate extremal dependence measures. This is the first work to explore statistical inference based on these probabilistic limit results. Our approach ensures self-consistent inference across the measures we consider, for the first time. In addition to this desirable feature, for individual extremal dependence measures, we show that our estimators are competitive with existing inferential methods.

2 Links between the sample cloud and extremal dependence measures

2.1 The limiting shape of a scaled sample cloud

A sample cloud corresponds to n independent samples from the joint distribution of (X_1, X_2) ; we denote this by $C_n = \{(X_{1,i}, X_{2,i}); i = 1, \dots, n\}$. The limiting convex hull of C_n , as $n \rightarrow \infty$, has been previously studied in the literature; see [Eddy and Gale \(1981\)](#), [Brozius and de Haan \(1987\)](#) and [Davis et al. \(1987\)](#). Following [Nolde and Wadsworth \(2022\)](#), our focus is on a scaled version of C_n , under certain conditions. Here, and throughout the paper, we assume that the variables (X_1, X_2) have standard exponential marginal distributions, i.e., $\Pr(X_i < x) = 1 - e^{-x}$, for $x \geq 0$ and $i = 1, 2$, and that their joint density, $f(x_1, x_2)$, exists. Consider a scaled random sample from the joint distribution of (X_1, X_2) , denoted by $C_n^* = \{(X_{1,i}, X_{2,i})/\log n; i = 1, \dots, n\}$. The $\log n$ scaling is chosen due to the exponential marginal distributions of X_1 and X_2 , as it ensures that $\max_{i=1, \dots, n} (X_{j,i}/\log n) \xrightarrow{p} 1$, as $n \rightarrow \infty$, for $j = 1, 2$; other light-tailed margins could also be used here and would result in different scaling functions being required.

Interest lies in studying the asymptotic shape of C_n^* , as $n \rightarrow \infty$. A useful tool in this task is the gauge function $g(x_1, x_2)$, defined via the relationship

$$-\log f(tx_1, tx_2) \sim tg(x_1, x_2), \quad t \rightarrow \infty, \quad x_1, x_2 \geq 0.$$

As $n \rightarrow \infty$, the scaled sample C_n^* converges onto the compact limit set

$$G^* = \{(x_1, x_2) : g(x_1, x_2) \leq 1\} \subseteq [0, 1]^2.$$

The set G^* is star-shaped, meaning that if $(x_1, x_2) \in G^*$, then $(tx_1, tx_2) \in G^*$ for all $t \in (0, 1)$. Throughout, we assume that the limit set G^* exists. In what follows, the boundary set

$$G = \{(x_1, x_2) : g(x_1, x_2) = 1\} \subset [0, 1]^2 \tag{2}$$

is of particular interest. The shapes of the limit set G^* and its boundary G are determined by the dependence between the variables, and would also alter under different marginal distributions.

In [Figure 1](#), we demonstrate the set G for four different copulas. We will use these distributions as examples throughout the paper. The first is a bivariate Gaussian copula with correlation parameter $\rho \in [0, 1]$. [Nolde \(2014\)](#) shows that the gauge function in this case has the form

$$g(x_1, x_2) = (1 - \rho^2)^{-1} \left(x_1 + x_2 - 2\rho x_1^{1/2} x_2^{1/2} \right), \quad x_1, x_2 \geq 0.$$

In the case of independence between the variables, i.e., when $\rho = 0$, the gauge function is simply $g(x_1, x_2) = x_1 + x_2$. For details on the calculation of the remaining three gauge functions discussed below, see [Simpson et al. \(2021\)](#). First, consider an inverted bivariate extreme value copula with logistic model and dependence parameter $\gamma \in (0, 1]$ (see [Ledford and Tawn, 1997](#)), with $\gamma = 1$ corresponding to complete independence, which has a gauge function of the form

$$g(x_1, x_2) = \left(x_1^{1/\gamma} + x_2^{1/\gamma} \right)^\gamma, \quad x_1, x_2 \geq 0,$$

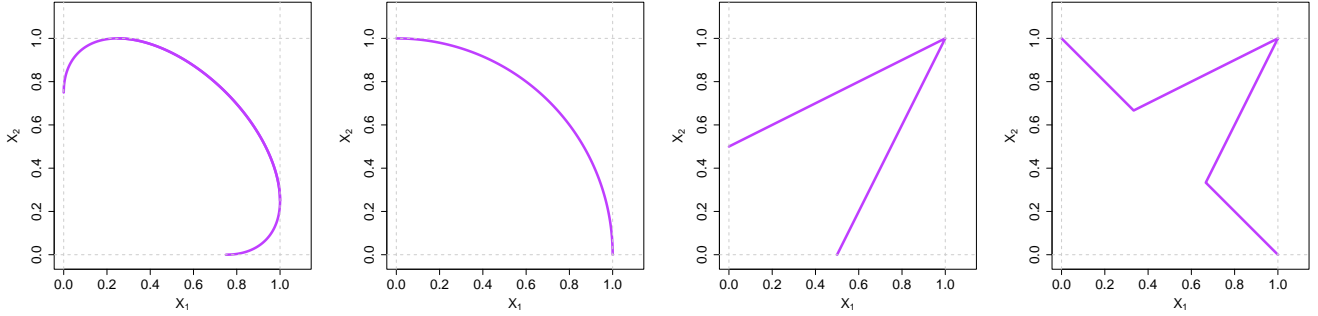


Figure 1: The boundary set G for Gaussian, inverted logistic, logistic and asymmetric logistic (left to right) dependence models with exponential margins. The Gaussian correlation parameter is set to $\rho = 0.5$, and the (inverted/asymmetric) logistic dependence parameter to $\gamma = 0.5$.

and a bivariate extreme value copula with logistic model (Gumbel, 1960), again with dependence parameter $\gamma \in (0, 1]$, having the gauge function

$$g(x_1, x_2) = \begin{cases} \frac{1}{\gamma} \max(x_1, x_2) - \left(\frac{1}{\gamma} - 1\right) \min(x_1, x_2), & x_1, x_2 \geq 0, \gamma < 1, \\ x_1 + x_2, & x_1, x_2 \geq 0, \gamma = 1. \end{cases}$$

There is a discontinuity here between $\gamma = 1$ and $\gamma \rightarrow 1$, which is linked to findings about the logistic model in Ledford and Tawn (1996); since $\gamma = 1$ corresponds to independence, which is already covered by the Gaussian copula with $\rho = 0$, we restrict to the $\gamma < 1$ case in the remainder of the paper.

The first two examples in Figure 1 are widely known to correspond to asymptotically independent models, while the third exhibits asymptotic dependence if $\gamma < 1$ (Coles et al., 1999). An important link between the bivariate gauge function and extremal dependence comes from the value of $g(1, 1)$ (Nolde, 2014). If $g(1, 1) < 1$, this corresponds to the case of asymptotic independence with $\chi = 0$, while under asymptotic dependence, with $\chi > 0$, we have $g(1, 1) = 1$. This is clearly satisfied by the three examples above. However, it is also possible to have $g(1, 1) = 1$ and $\chi = 0$, so care with interpretation is needed.

Finally, we consider a bivariate extreme value copula with asymmetric logistic model (Tawn, 1988), where a mixture of extremal dependence features is possible, arising from logistic and independence components. That is, both variables can be simultaneously extreme, putting this model in the asymptotic dependence class, but each of the variables can also be individually large while the other is of smaller order. We provide details on the form of this dependence model in Appendix A. Following the discussion of discontinuity in the logistic model above, we again restrict the dependence parameter to $\gamma \in (0, 1)$. Moreover, setting the additional model parameters to $\theta_1 = \theta_2 = 0$ yields a logistic model, while setting $\theta_1 = \theta_2 = 1$ recovers the setting of independence; we therefore focus on $\theta_1, \theta_2 \in (0, 1)$ in the following. Figure 1 (right panel) also shows the gauge function of this copula, which is of the form

$$g(x_1, x_2) = \min \left\{ (x_1 + x_2); \frac{1}{\gamma} \max(x_1, x_2) - \left(\frac{1}{\gamma} - 1\right) \min(x_1, x_2) \right\}, \quad x_1, x_2 \geq 0. \quad (3)$$

Here, we once again have $\chi > 0$ and it is clear that $g(1, 1) = 1$. Interestingly, the gauge function does not depend on the parameters θ_1 and θ_2 when $\theta_1, \theta_2 \in (0, 1)$.

2.2 Bivariate extremal dependence features

We now introduce the tail dependence features that we aim to estimate, beginning with the coefficient of asymptotic independence, η , of [Ledford and Tawn \(1996\)](#), or equivalently $\bar{\chi} = 2\eta - 1$ ([Coles et al., 1999](#)). Recall that we assume the variables X_1 and X_2 have standard exponential marginal distributions. Then, $\eta \in (0, 1]$ is defined by considering the behaviour of the joint survivor function

$$\Pr(X_1 > x, X_2 > x) \sim \mathcal{L}(e^x)e^{-x/\eta},$$

as $x \rightarrow \infty$, where the function \mathcal{L} is slowly varying at infinity. Considering the definition of χ in (1), when $\eta = 1$, this yields $\chi = \lim_{x \rightarrow \infty} \mathcal{L}(e^x)$, whereas if $\eta < 1$, we obtain $\chi = \lim_{x \rightarrow \infty} \mathcal{L}(e^x)e^{-(1/\eta-1)x} = 0$. Hence, for $\eta = 1$ and $\mathcal{L}(x) \not\rightarrow 0$ as $x \rightarrow \infty$, we have $\chi > 0$, and therefore asymptotic dependence. If $\eta < 1$, or $\eta = 1$ and $\mathcal{L}(x) \rightarrow 0$ as $x \rightarrow \infty$, we have $\chi = 0$ and the variables are asymptotically independent. Estimation of the coefficient η can contribute towards the classification of tail dependence behaviour in practice, and in turn enable the selection of an appropriate model for the joint extremes.

[Wadsworth and Tawn \(2013\)](#) extend the approach of [Ledford and Tawn \(1996\)](#) by allowing for different scalings. To achieve this, they consider limiting probabilities of the form

$$\Pr\{X_1 > \omega x, X_2 > (1 - \omega)x\} \sim \mathcal{L}_\omega(e^x)e^{-x\lambda(\omega)},$$

as $x \rightarrow \infty$, for $\omega \in [0, 1]$, $\lambda(\omega) \in (0, 1]$ and some \mathcal{L}_ω that is slowly varying at infinity. The case where $\omega = 1/2$ is linked to the coefficient η by the relation $\eta^{-1} = 2\lambda(1/2)$. Under asymptotic dependence, we therefore have $\lambda(1/2) = 1/2$, and more generally, for $\omega \in [0, 1]$, we have $\lambda(\omega) = \max(\omega, 1 - \omega)$ in this case. Under complete independence, $\lambda(\omega) = 1$ for all $\omega \in [0, 1]$.

Motivated by the possibility of mixture structures in the extremal dependence features, [Simpson et al. \(2020\)](#) introduced a further set of indices related to η . They consider a separate measure for each subset of variables, which describes whether they can be simultaneously large while the other variables are of smaller order. In the bivariate case, there are two measures of interest, denoted by $\tau_1(\delta), \tau_2(\delta) \in (0, 1]$, for $\delta \in [0, 1]$. The measure $\tau_1(\delta)$ is based on a hidden regular variation assumption, see [Simpson et al. \(2020\)](#) and [Nolde and Wadsworth \(2022\)](#), and in exponential margins is defined by the relation

$$\Pr(X_1 > x, X_2 \leq \delta x) \sim \mathcal{L}_\delta(e^x)e^{-x/\tau_1(\delta)}, \quad (4)$$

as $x \rightarrow \infty$, for $\delta \in [0, 1]$ and some slowly varying function \mathcal{L}_δ . The function $\tau_1(\delta)$ is monotonically increasing with δ , and has $\tau_1(1) = 1$. If there exists any $\delta^* < 1$ such that $\tau_1(\delta^*) = 1$, the variable X_1 can take its largest values while X_2 is of smaller order, otherwise X_1 can only take its largest values when X_2 is also large. The measure $\tau_2(\delta)$ can be defined analogously through the limiting behaviour of $\Pr(X_1 \leq \delta x, X_2 > x)$, as $x \rightarrow \infty$.

Finally, we consider the conditional extremes modelling approach of [Heffernan and Tawn \(2004\)](#). Conditional extremes models capture both asymptotic dependence and asymptotic independence, so are widely applicable. The conditional extremes framework requires that the marginal distributions have

Dependence model	η	$\lambda(\omega)$	$\tau_1(\delta) = \tau_2(\delta)$	$\alpha_1 = \alpha_2$	$\beta_1 = \beta_2$
Gaussian	$(1 + \rho)/2$	$\begin{cases} \frac{1-2\rho\{\omega(1-\omega)\}^{1/2}}{1-\rho^2}, & \text{if } t_\omega \geq \rho^2 \\ \max(\omega, 1-\omega), & \text{if } t_\omega < \rho^2 \end{cases}$	$\begin{cases} 1, & \text{if } \delta \geq \rho^2 \\ \frac{1-\rho^2}{1+\delta-2\rho\delta^{1/2}}, & \text{if } \delta < \rho^2 \end{cases}$	ρ^2	$1/2$
Inverted logistic	$2^{-\gamma}$	$\{\omega^{1/\gamma} + (1-\omega)^{1/\gamma}\}^\gamma$	1	0	$1 - \gamma$
Logistic	1	$\max(\omega, 1-\omega)$	$\gamma/(1 + \gamma\delta - \delta)$	1	0
Asymmetric logistic	1	$\max(\omega, 1-\omega)$	1	1	0

Table 1: Values of the set of extremal dependence coefficients $\{\eta, \lambda(\omega), \tau_1(\delta), \tau_2(\delta), \alpha_1, \alpha_2, \beta_1, \beta_2\}$ for a Gaussian model with correlation parameter $\rho \in [0, 1]$ and (inverted) logistic models with dependence parameter $\gamma \in (0, 1)$. Here, $t_\omega = \min(\omega, 1 - \omega) / \max(\omega, 1 - \omega)$.

exponential upper tails, which is clearly satisfied when (X_1, X_2) have standard exponential margins. Selecting X_1 as the conditioning variable, we assume there exist functions $a_1(\cdot)$ and $b_1(\cdot) > 0$ such that

$$\left\{ \frac{X_2 - a_1(X_1)}{b_1(X_1)}, X_1 - u \right\} \Big| X_1 > u \rightarrow (Z, E), \quad \text{as } u \rightarrow \infty, \quad (5)$$

where $E \sim Exp(1)$ is independent of Z , and Z represents some non-degenerate residual distribution that places no mass on $\{+\infty\}$ (Heffernan and Tawn, 2004; Keef et al, 2013). Under this conditioning, a suitably normalised version of X_2 and exceedances of X_1 above the threshold u become independent as $u \rightarrow \infty$. Heffernan and Tawn (2004) propose setting $a_1(x) = \alpha_1 x$ and $b_1(x) = x^{\beta_1}$, for $\alpha_1 \in [0, 1]$ and $\beta_1 \in [0, 1)$, and demonstrate that this is a reasonable choice for a range of non-negatively dependent distributions. The case where $\alpha_1 = 1$ and $\beta_1 = 0$ corresponds to asymptotic dependence, while $\alpha_1 < 1$ corresponds to asymptotic independence, with complete independence achieved when $\alpha_1 = 0$, $\beta_1 = 0$ and $Z \sim Exp(1)$. An analogous result holds if X_2 is selected as the conditioning variable instead, with normalising functions $a_2(x) = \alpha_2 x$ and $\beta_2(x) = x^{\beta_2}$ for $\alpha_2 \in [0, 1]$ and $\beta_2 \in [0, 1)$.

The values of η , $\lambda(\omega)$, $\tau_1(\delta)$, $\tau_2(\delta)$, α_1 , α_2 , β_1 and β_2 for the distributions considered in Figure 1 are given in Table 1. For the first three cases, it is clear that the symmetry of the models means we have $\tau_1(\delta) = \tau_2(\delta)$, $\alpha_1 = \alpha_2$ and $\beta_1 = \beta_2$ in each case. In Section 2.3, we will see that these equivalences also arise when G is symmetric about the line $x_1 = x_2$, even if the distribution itself is not symmetric, as in the asymmetric logistic case when $\theta_1 \neq \theta_2$. For the Gaussian distribution, the $\tau_i(\delta)$ ($i = 1, 2$) result for $\delta < \rho^2$ was derived by Nolde and Wadsworth (2022). In Section 2.3, we explain how each of these features is linked to the set G , using results from Nolde and Wadsworth (2022).

2.3 Geometric interpretation of bivariate extremal dependence features

Balkema and Nolde (2010) were the first to provide results linking the asymptotic shape of a scaled sample cloud to asymptotic independence. Nolde (2014) extended this work to show that the coefficient of asymptotic independence, η , is linked to the set G defined in (2) via the relationship

$$\eta = \min \{s \in (0, 1] : [s, \infty]^2 \cap G = \emptyset\}. \quad (6)$$

We can think of this as moving the set $[1, \infty]^2$ along the line $x_2 = x_1$ towards the origin, until it intersects the set G (although this intersection does not have to occur on the diagonal). We demonstrate this feature

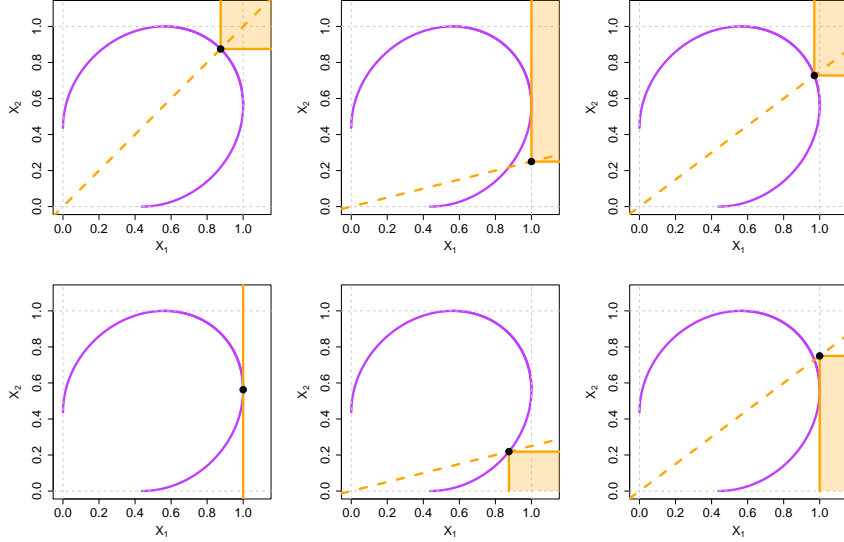


Figure 2: Examples of the set G (purple) and demonstration of calculating η , $\lambda(4/5)$, $\lambda(4/7)$, $\tau_1(3/4)$, $\tau_1(1/4)$ and α_1 (clockwise from top left) for a Gaussian model with correlation parameter $\rho = 0.75$. Top left: the set $[\eta, \infty]^2$ (orange region), and the point (η, η) (black circle) which lies on $x_2 = x_1$ (orange dashed line). Top, centre and right: the sets $s_\omega S_\omega$ (orange regions) for $\omega = 4/5, 4/7$, and the points $(s_\omega, \frac{1-\omega}{\omega}s_\omega)$ (black circles), lying on $x_2 = \frac{1-\omega}{\omega}x_1$ (orange dashed line). Bottom, right and centre: the sets $\tau_1(\delta)S_{1,\delta}$ (orange regions), for $\delta = 3/4, 1/4$, and the points $(\tau_1(\delta), \delta\tau_1(\delta))$ (black circles), lying on $x_2 = \delta x_1$ (orange dashed line). Bottom left: the line $x_1 = 1$ (orange) and the point $(1, \alpha_1)$ (black circle).

in the top left panel of Figure 2 for a Gaussian copula with $\rho = 0.75$. In this case, $\eta = (1 + \rho)/2 = 0.875$, corresponding to the known value of η for this model. A higher dimensional version of (6) was previously used by Simpson et al. (2021) to study the extremal dependence structure of vine copulas.

To calculate the value of $\lambda(\omega)$, Nolde and Wadsworth (2022) consider sets of the form

$$S_\omega = \{(x_1, x_2) : x_1 > \omega / \max(\omega, 1 - \omega), x_2 > (1 - \omega) / \max(\omega, 1 - \omega)\}, \quad \omega \in [0, 1].$$

They prove that

$$\lambda(\omega) = \frac{\max(\omega, 1 - \omega)}{s_\omega}, \quad \text{with } s_\omega = \min \{s \in [0, 1] : sS_\omega \cap G = \emptyset\}. \quad (7)$$

The set $S_{1/2}$ is equivalent to $[1, \infty]^2$, so that the value of $s_{1/2}$ is η , as we expect since $\lambda(1/2) = 1/(2\eta)$, as discussed in Section 2.2. The central and right panels of the top row of Figure 2 demonstrate the sets $s_\omega S_\omega$ for the Gaussian copula with $\rho = 0.75$, taking $\omega = 4/5, 4/7$, respectively. This highlights the need to consider the whole set S_ω when deducing $\lambda(\omega)$, not just the vertex $x_2 = \frac{1-\omega}{\omega}x_1$. When $\omega = 4/5$, the intersection of G and $s_\omega S_\omega$ occurs on the edge of the rectangle, with $s_\omega = 1$ and $\lambda(\omega) = \max(\omega, 1 - \omega) = 4/5$. In contrast, for $\omega = 4/7$, the intersection does occur on the line $x_2 = \frac{1-\omega}{\omega}x_1$, with the value of $\lambda(4/7)$ given by the first Gaussian $\lambda(\omega)$ case in Table 1.

Nolde and Wadsworth (2022) link the set G to $\tau_1(\delta)$ and $\tau_2(\delta)$ by considering sets

$$S_{1,\delta} = \{(x_1, x_2) : x_1 \in (1, \infty], x_2 \in [0, \delta]\}, \quad S_{2,\delta} = \{(x_1, x_2) : x_1 \in [0, \delta], x_2 \in (1, \infty]\},$$

for $\delta \in [0, 1]$, and showing that

$$\tau_i(\delta) = \min \{s \in (0, 1] : sS_{i,\delta} \cap G = \emptyset\}, \quad (8)$$

for $i = 1, 2$. In a similar way to the η representation of [Nolde \(2014\)](#), we can think of $\tau_1(\delta)$ as taking the set $S_{1,\delta}$ and moving it along the line $x_2 = \delta x_1$ towards the origin until it intersects the set G (where the intersection does not necessarily occur on the line $x_2 = \delta x_1$). This is demonstrated in the right and central panels of the bottom row of [Figure 2](#) for the Gaussian model with $\rho = 0.75$, taking $\delta = 0.75, 0.25$, respectively. We have $\tau_1(0.75) = 1$, and $\tau_1(0.25) < 1$, with its exact form given in [Table 1](#).

Finally, in the conditional extremes framework, [Nolde and Wadsworth \(2022\)](#) show that

$$\alpha_1 = \max \{\tilde{\alpha}_1 \in [0, 1] : g(1, \tilde{\alpha}_1) = 1\}. \quad (9)$$

It is possible to have more than one such $\tilde{\alpha}_1$, but the largest value is needed to avoid Z in [\(5\)](#) placing mass on $\{+\infty\}$. This means we should find the largest value of x_2 where G intersects the line $x_1 = 1$. Considering an analogous definition of α_2 , alongside result [\(6\)](#), it is clear that $\eta \geq \max(\alpha_1, \alpha_2)$. If there are ν separate values of $\tilde{\alpha}_1$ in [\(9\)](#), this indicates a ν -component mixture structure in the extremal dependence conditioning on X_1 large, following the representation of [Tendijck et al. \(2022\)](#). Moreover, the smallest value of δ such that $\tau_1(\delta) = 1$ is given by $\delta^* = \min \{\tilde{\alpha}_1 \in [0, 1] : g(1, \tilde{\alpha}_1) = 1\}$. If $\nu = 1$ with only one value of $\tilde{\alpha}_1$ satisfying $g(1, \tilde{\alpha}_1) = 1$, we have $\delta^* = \alpha_1$; this is the case in the bottom left panel of [Figure 2](#) for our Gaussian example with $\rho = 0.75$, where $\alpha_1 = \rho^2 = 0.75^2$. The asymmetric logistic example in [Figure 1](#) has $\nu = 2$ and $\tilde{\alpha}_1 \in \{0, 1\}$, yielding $\alpha_1 = 1$ and $\delta^* = 0$. Overall, the set of measures $\{\eta, \max_{\delta < 1} \tau_1(\delta), \max_{\delta < 1} \tau_2(\delta)\}$ can describe whether the variables (X_1, X_2) can be simultaneously large, whether one variable is large while the other is of smaller order, or whether we have a combination of these cases, but considering the $\tilde{\alpha}_1$ values from [\(9\)](#) can provide additional insight.

[Nolde and Wadsworth \(2022\)](#) also present results on the parameter β_1 in the conditional extremes model, linked to the rate at which $g(1, \alpha_1 + u) \rightarrow 1$ as $u \rightarrow 0$. In particular, they show that

$$g(1, \alpha_1 + u) = 1 + O \left\{ u^{1/(1-\beta)} \right\}, \quad \text{as } u \rightarrow 0. \quad (10)$$

The results for α_2 and β_2 are analogous to those presented here.

As well as considering how the extremal dependence features described above can be obtained from the set G , we examine how much information these features can give us about G . The indices $\lambda(\omega)$, $\tau_1(\delta)$ and $\tau_2(\delta)$ ($\omega, \delta \in [0, 1]$) are the most interesting from this perspective, as collectively they can sometimes fully describe G . In the logistic case, only $\tau_1(\delta)$ and $\tau_2(\delta)$ are needed; the opposite is true for the inverted logistic case; whereas for the Gaussian case, they are all required. However, for the asymmetric logistic model, the extremal dependence mixture structure means that collectively, $\lambda(\omega)$ and $\tau_i(\delta)$ ($i = 1, 2$) do not provide sufficient information for us to deduce the shape of G . Hence, there is value in developing an approach to estimate G directly, to enhance our understanding of the nature of the extremal dependence, as well as for deducing self-consistent estimates of currently studied extremal dependence features. The remainder of the paper is dedicated to this goal.

3 Estimation of the limit set G

3.1 Framework for modelling the boundary set G

We require the variables (X_1, X_2) to have exponential margins, which can be achieved in practice by applying rank and probability integral transforms to each variable. Suppose we have n observations of the random variables Y_i , $i = 1, 2$, denoted by $y_{i,1}, \dots, y_{i,n}$. The approximate transformation to observations of X_i with exponential margins is given by

$$x_{i,j} = -\log \left\{ 1 - \frac{\text{rank}(y_{i,j})}{n+1} \right\}, \quad (11)$$

for $i = 1, 2$ and $j = 1, \dots, n$; an alternative version of this transformation with a parametric form for the tail is detailed in [Coles and Tawn \(1991\)](#). Applying transformation (11) as a preliminary step allows us to focus on estimating the extremal dependence features. We consider (X_1, X_2) in terms of the pseudo-polar coordinates (R, W) , with

$$R = X_1 + X_2 > 0, \quad W = X_1/R \in [0, 1],$$

which we refer to as radial and angular components, respectively. Due to our choice of marginal distribution, these are not the same as the radial and angular components on Fréchet or Pareto scale used by [Resnick \(1987\)](#) or [Coles and Tawn \(1991\)](#), for instance, but are akin to those in [Wadsworth and Tawn \(2013\)](#). This polar coordinate formulation lends itself to estimating G since the star-shaped nature of the set G^* means that any ray emanating from the origin, i.e., corresponding to a fixed angle $w \in [0, 1]$, must intersect the set G exactly once. We are therefore interested in the largest possible radial value associated with each angle w , after the $\log n$ scaling of (X_1, X_2) , which also induces $\log n$ scaling of R . In practice, having a finite amount of data means that observations of $(X_1, X_2)/\log n$ are not restricted to the set $[0, 1]^2$, unlike the set G that we aim to estimate, and the distribution of the observed radial variable need not have a finite upper endpoint. We propose to estimate G by estimating high quantiles of the distribution of $R \mid W = w$ for all $w \in [0, 1]$, then transforming these estimates to the original coordinates (X_1, X_2) via the relations $X_1 = RW$, $X_2 = R(1 - W)$ and finally scaling them onto $[0, 1]^2$.

A natural candidate for modelling the tail of $R \mid W = w$ is the generalised Pareto distribution (GPD) ([Davison and Smith, 1990](#)). That is, for $w \in [0, 1]$ and a suitable threshold u_w , we have

$$\Pr(R < r \mid R > u_w, W = w) = 1 - \left[1 + \xi(w) \left\{ \frac{r - u_w}{\sigma(w)} \right\} \right]_+^{-1/\xi(w)}, \quad (12)$$

for $r > u_w$, $x_+ = \max\{x, 0\}$, scale parameter $\sigma(w) > 0$ and shape parameter $\xi(w) \in \mathbb{R}$. We consider $r_q(w)$, a high quantile of the distribution of $R \mid W = w$, for all $w \in [0, 1]$, such that

$$\Pr\{R < r_q(w) \mid W = w\} = q,$$

with $r_q(w) > u_w$. For $\xi(w) \neq 0$, this quantity is given by

$$r_q(w) = u_w + \frac{\sigma(w)}{\xi(w)} \left[\left\{ \frac{\zeta_u(w)}{1 - q} \right\}^{\xi(w)} - 1 \right], \quad (13)$$

where $\zeta_u(w) = \Pr(R > u_w \mid W = w)$. We aim to estimate the set $\{(r_q(w), w) : w \in [0, 1]\}$ for q close to 1.

3.2 Estimation of G : a local approach

Suppose we have n observations of the radial-angular components (R, W) , denoted by $(r_1, w_1), \dots, (r_n, w_n)$. If (X_1, X_2) have a joint density, we will not observe repeated observations of the angular component in a finite sample, so for any given $w \in [0, 1]$, we will not have sufficient observations¹ to fit distribution (12) directly. We propose a two-step approach to address this issue. First, we obtain local estimates of the model parameters $\sigma(w)$ and $\xi(w)$ and corresponding radial quantiles $r_q(w)$ for fixed values of w . From these, we construct a local estimate of the set G , which we denote \hat{G}^L . The theoretical examples in Figure 1 showed that the set G may generally be smooth, but can have points of non-differentiability. Motivated by this observation, our second step, detailed in Section 3.3, exploits the framework of generalised additive models (GAMs) to provide smooth estimates of the GPD threshold and scale parameter, and hence of $r_q(w)$, for $w \in [0, 1]$. In Section 3.3, we explain how we use \hat{G}^L to inform the choice of spline basis functions in the GAM framework and yield an estimate \hat{G} of G .

In the local estimation procedure, we use observed radial values corresponding to the angular components in some neighbourhood of w , defined as

$$\mathcal{R}_w = \{r_i : |w_i - w| \leq \epsilon_w, i \in \{1, \dots, n\}\}, \quad (14)$$

for some $\epsilon_w > 0$, to be equivalent to the event $W = w$, i.e., this requires the GPD parameters to be approximately constant over \mathcal{R}_w . Using standard maximum likelihood estimation techniques with observations from \mathcal{R}_w , it is straightforward to estimate the parameters $\sigma(w)$, $\xi(w)$ in (12) and (13), and we suggest setting $\zeta_u(w) = q_u \in [0, q]$ identically for all w with the corresponding threshold u_w estimated empirically. We propose to carry out this estimation at a range of angular values, denoted by w_1^*, \dots, w_k^* , and use these to estimate the radial quantiles in (13), denoting these quantile estimates by $\hat{r}_q(w_j^*)$, $j \in J_k := \{1, \dots, k\}$. The w_j^* values are not required to belong to the set of observed W values and may be selected so that the associated $\mathcal{R}_{w_j^*}$ sets overlap. As well as k and the values w_j^* ($j \in J_k$), other tuning parameters to be selected here are the quantile levels (q_u, q) and the neighbourhood sizes $\epsilon_{w_j^*}$. We discuss our approach to choosing these quantities in the Supplementary Material (Simpson and Tawn, 2022), where we propose choosing $\epsilon_{w_j^*}$ separately for each j to ensure $|\mathcal{R}_{w_j^*}| = m$. Our default tuning parameter suggestions are $k = 199$, $m = 100$, $q_u = 0.5$ and $q = 0.999$.

To obtain an estimate of G , denoted \hat{G}^L for the local approach, we first transform the local radial quantile estimates back to the original (X_1, X_2) coordinates by setting

$$\tilde{x}_{1,j} = \hat{r}_q(w_j^*) \cdot w_j^*, \quad \tilde{x}_{2,j} = \hat{r}_q(w_j^*) \cdot (1 - w_j^*), \quad j \in J_k.$$

To ensure $G \subset [0, 1]^2$, a naive approach would be to simply divide each component by its largest value, i.e., by updating to $\tilde{x}'_{i,j} = \tilde{x}_{i,j} / \max_{j \in J_k} \tilde{x}_{i,j}$, $i = 1, 2$. However, this is strongly influenced by the largest estimates, and does not work well in practice. Instead, we suggest a two-step scaling/truncation approach, initially informed by an existing estimator of η and then corrected to take into account known features of G . We begin by scaling all $(\tilde{x}_{1,j}, \tilde{x}_{2,j})$ values to obtain a preliminary local limit set estimate $\hat{G}_\eta^L =$

¹The rank transformation given in (11) means that a small number of repetitions are possible.

$\{(\hat{x}_{1,j}^{G_\eta}, \hat{x}_{2,j}^{G_\eta}) : j \in J_k\}$, with the scaling factor chosen so that an estimate of η from the resulting set would match the Hill estimator $\hat{\eta}_H$, see (20), that will be introduced in Section 4.4, i.e., so that \hat{G}_η^L and $[\hat{\eta}_H, \infty]^2$ just intersect. The scaling factor that achieves this is

$$x^* = \hat{\eta}_H \left[\max_{j \in J_k} \{ \min(\tilde{x}_{1,j}, \tilde{x}_{2,j}) \} \right]^{-1},$$

i.e., we set $\hat{x}_{i,j}^{G_\eta} = x^* \tilde{x}_{i,j}$ for $i = 1, 2, j \in J_k$. The resulting estimate \hat{G}_η^L is not guaranteed to lie within $[0, 1]^2$, nor to intersect the lines $x_1 = 1$ and $x_2 = 1$; the second step corrects for these possibilities, taking each of the arguments separately. In step 2a, for $i = 1, 2$, if $\max_{j \in J_k} \hat{x}_{i,j}^{G_\eta} \geq 1$, we truncate by defining $\hat{x}_{i,j}^G = \min\{1, \hat{x}_{i,j}^{G_\eta}\}$, $j \in J_k$. Alternatively, in step 2b, if $\max_{j \in J_k} \hat{x}_{i,j}^{G_\eta} < 1$, we ensure that our estimate of G intersects the line $x_i = 1$ at least once by dividing the component by its maximum value, setting $\hat{x}_{i,j}^G = \hat{x}_{i,j}^{G_\eta} / \max_{\ell \in J_k} \hat{x}_{i,\ell}^{G_\eta}$. The scaling in step 2b means that an estimate of η obtained from \hat{G}^L (as will be discussed in Section 4.2) may not be exactly equal to $\hat{\eta}_H$, but our approach actually improves the estimates of this coefficient in cases where $\hat{\eta}_H$ has a tendency to underestimate, such as under asymptotic dependence in the logistic model. This will be demonstrated through simulations in Section 5.1. The scaling/truncation approach is demonstrated pictorially in Simpson and Tawn (2022).

3.3 Estimation of G : a smoothed approach

There is no guarantee of smoothness in the estimated set \hat{G}^L , whatever the choice of tuning parameters. As we have already identified, it may be desirable to impose that our estimator of G is smooth, at least for some subsets of $w \in [0, 1]$. To achieve this, we use \hat{G}^L to inform a ‘smoothing’ method for the GPD parameters in the second step of our procedure. In particular, we follow the approach of Youngman (2019) by first carrying out quantile regression to estimate the thresholds u_w at the same quantile level $q_u \in [0, q]$ as in Section 3.2 by exploiting the asymmetric Laplace distribution (Yu and Moyeed, 2001). The parameters of the asymmetric Laplace distribution are modelled using generalised additive models (GAMs). We find that applying this quantile regression approach to R often gives impossible negative estimates near the largest and smallest observed angles. We overcome this issue by working with $\log R$ in this step, and then back-transform to obtain the required radial threshold estimates. For exceedances above u_w , we also assume that the parameter values in the GPD vary smoothly with the value of $w \in [0, 1]$. Again following the approach of Youngman (2019), we adopt a GAM form for the log-scale parameter. Both parts of this approach are implemented in the R package `evgam` (Youngman, 2020). The shape parameter could analogously be allowed to vary smoothly, but this is notoriously difficult to estimate and we found that in tests, anything other than assuming a constant value resulted in increased variance without reducing the bias of our estimates.

We allow the GAM form for the model parameters to be linear, quadratic or cubic B-splines, with κ knots; for simplicity, the same spline degree and knot positions are chosen for u_w and $\log \sigma(w)$, and corresponding estimates of the quantiles in (13). Once we have estimates of the high radial quantiles, the procedure to obtain an estimate of G is via transformation and scaling/truncation, equivalent to that for \hat{G}^L . Although, theoretically, this approach allows for estimates of G across the full range $w \in [0, 1]$,

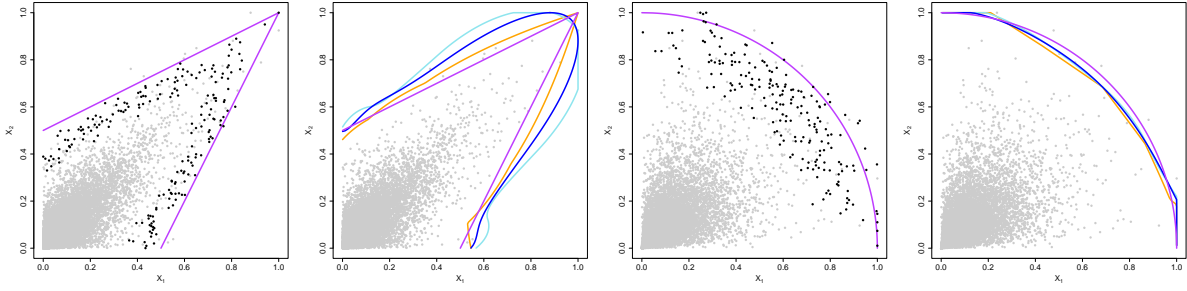


Figure 3: Left: logistic data scaled by $\log n$, with the true set G (purple) and \hat{G}^L (black points). Left-centre: the estimated sets \hat{G}^{S_1} (orange), \hat{G}^{S_2} (light blue) and \hat{G}^{S_3} (dark blue), taking $k = 199$, $m = 100$, $q_u = 0.5$, $q = 0.9$ and $\kappa = 7$. Right-centre and right: equivalent plots for inverted logistic data.

outside the observed angles these can be unreliable, and we restrict our estimates to the observed range, $w \in (w^m, w^M)$. The resulting estimates of G are denoted by \hat{G}^{S_1} , \hat{G}^{S_2} and \hat{G}^{S_3} for the linear, quadratic and cubic splines, respectively.

Considering different spline degrees here is useful, as it enables us to capture different shapes of G . To choose between the estimators \hat{G}^{S_1} , \hat{G}^{S_2} and \hat{G}^{S_3} , we select the spline degree where the estimated radial quantiles at the angles w_j^* ($j \in J_k$) are closest to those from the local procedure, when compared using the mean absolute error. This selection criterion is a reasonable choice, since by forcing an equal number of points in each set $\mathcal{R}_{w_j^*}$, we have ensured there will be approximately the same uncertainty in each radial estimate. The selected estimator \hat{G} (from \hat{G}^{S_1} , \hat{G}^{S_2} or \hat{G}^{S_3}) becomes our preferred option for modelling G . That is, letting $\hat{r}_q^L(w_j^*)$, $j \in J_k$, denote the local radial quantile estimates and $\hat{r}_q^{S_d}(w_j^*)$, $d = 1, 2, 3$, denote the corresponding estimates of $r_q(w_j^*)$ for \hat{G}^{S_d} , we have

$$\hat{G} = \left\{ \hat{G}^{S_d} : d = \arg \min_{d^* \in \{1,2,3\}} \sum_{j \in J_k} |\hat{r}_q^L(w_j^*) - \hat{r}_q^{S_{d^*}}(w_j^*)| \right\}. \quad (15)$$

Figure 3 gives a demonstration of the full approach for 10,000 simulated values from a bivariate extreme value model with a logistic model and parameter $\gamma = 1/2$, and its inverted counterpart, with comparison to the true sets G . The tuning parameters here are chosen for illustrative purposes. It is clear that \hat{G}^L is not smooth and tends to underestimate G , whereas \hat{G}^{S_1} , \hat{G}^{S_2} and \hat{G}^{S_3} offer varying levels of improvement. The linear spline performs the best in the logistic case where G has a pointed shape, with the mean absolute errors evaluated in (15) being 55.23, 67.37 and 57.64 for \hat{G}^{S_1} , \hat{G}^{S_2} and \hat{G}^{S_3} , respectively, so $\hat{G} = \hat{G}^{S_1}$. The errors in the inverted logistic case are 61.95, 61.50 and 61.29, i.e., the cubic spline is slightly preferred as G is smooth, so $\hat{G} = \hat{G}^{S_3}$.

The smoothing method requires the introduction of further tuning parameters in our method, in the choice of κ and the position of the knots. Tuning parameter selection is discussed in detail in [Simpson and Tawn \(2022\)](#), where we suggest a default choice $\kappa = 7$, in addition to the suggested tuning parameters given for \hat{G}^L in Section 3.2. Knot-placement and the positions of w_j^* ($j \in J_k$), as well sensitivity to the extrapolation quantile q , are also discussed in [Simpson and Tawn \(2022\)](#), while we illustrate limited sensitivity to κ for an asymmetric logistic copula in Section 5.2.

4 Estimation of extremal dependence properties

4.1 Overview

Further exploiting the new procedure to estimate G , in Section 4.2, we now obtain estimates of η , $\lambda(\omega)$, $\tau_1(\delta)$, $\tau_2(\delta)$, α_1 and α_2 in a unified way. Due to the subtlety of result (10) for the conditional extremes parameters β_1 and β_2 , we choose not to estimate this as part of our self-consistent approach. Instead, we fix the corresponding α_i parameter to its estimated value, and then carry out inference for β_i ; this is discussed in Section 4.3. In Section 4.4, we discuss a range of techniques that are currently available to separately estimate the extremal dependence features that we consider. We compare the performance of each of these methods to that of our estimation approach in Section 5.

4.2 Exploiting the estimate \hat{G} for parameter estimation

For the estimation of the dependence properties discussed in this section, we consider \hat{G} in (15) at a finite number of angles, to facilitate the implementation. We choose these as identical to the w_j^* , $j \in J_k$, used in the local estimate \hat{G}^L , now denoting $\hat{G} = \{(\hat{x}_{1,j}^G, \hat{x}_{2,j}^G) : j \in J_k\}$. To estimate η using \hat{G} , we first note that result (6) from Nolde (2014) can be written as

$$\eta = \min \{s \in (0, 1] : G \cap [s, \infty]^2 = \emptyset\} = \max \{s \in (0, 1] : G \cap [s, \infty]^2 \neq \emptyset\}. \quad (16)$$

If we consider each point in our set \hat{G} to be a candidate for the intersection of G and $[\eta, \infty]^2$ required in (16), we can examine a corresponding set $[s_j^*, \infty]^2$ for each of these points by setting $s_j^* = \min(\hat{x}_{1,j}^G, \hat{x}_{2,j}^G)$. Then the resulting estimate of η is given by $\max(s_1^*, \dots, s_k^*)$, i.e.,

$$\hat{\eta}_G = \max_{j \in J_k} \{ \min(\hat{x}_{1,j}^G, \hat{x}_{2,j}^G) \}. \quad (17)$$

We estimate $\lambda(\omega)$, $\omega \in [0, 1]$, via estimation of s_ω in (7). We have

$$s_\omega = \min \{s \in [0, 1] : sS_\omega \cap G = \emptyset\} = \max \{s \in [0, 1] : sS_\omega \cap G \neq \emptyset\},$$

with $S_\omega = \{(x_1, x_2) : x_1 > \omega / \max(\omega, 1 - \omega), x_2 > (1 - \omega) / \max(\omega, 1 - \omega)\}$. Analogously to $\hat{\eta}_G$, we obtain candidate values $s_{\omega,j}^* = \max(\omega, 1 - \omega) \cdot \min\{\hat{x}_{1,j}^G / \omega, \hat{x}_{2,j}^G / (1 - \omega)\}$ for $j \in J_k$, with the resulting estimator

$$\hat{\lambda}_G(\omega) = \left[\max_{j \in J_k} \left\{ \min \left(\frac{\hat{x}_{1,j}^G}{\omega}, \frac{\hat{x}_{2,j}^G}{1 - \omega} \right) \right\} \right]^{-1}, \quad \omega \in [0, 1].$$

Next, consider the dependence measure $\tau_1(\delta)$. Result (8) gives that for $\delta \in [0, 1]$,

$$\tau_1(\delta) = \min \{s \in [0, 1] : (s, \infty) \times [0, \delta s] \cap G = \emptyset\} = \max \{s \in [0, 1] : (s, \infty) \times [0, \delta s] \cap G \neq \emptyset\}.$$

Our candidate points for the intersection of the sets G and $(\tau_1(\delta), \infty) \times [0, \delta \tau_1(\delta)]$ are all our estimated points on G where $\hat{x}_2^G \leq \delta \hat{x}_1^G$. Our estimate of $\tau_1(\delta)$ corresponds to the largest such value of \hat{x}_1^G . That is,

$$\hat{\tau}_{G,1}(\delta) = \max \{ \hat{x}_{1,j}^G : \hat{x}_{2,j}^G \leq \delta \hat{x}_{1,j}^G, j \in \{1, \dots, k\} \}.$$

Finally, for the conditional extremes parameter α_1 , results in [Nolde and Wadsworth \(2022\)](#) lead to

$$\hat{\alpha}_{G,1} = \max \left(\hat{x}_{2,j}^G : \hat{x}_{1,j}^G = 1, j \in \{1, \dots, k\} \right). \quad (18)$$

Due to our method of scaling onto $[0, 1]^2$, in practice there may only be exactly one value of $\hat{x}_{1,j}^G$ that is equal to one. The estimators of $\hat{\tau}_{G,2}(\delta)$ and $\hat{\alpha}_{G,2}$ are defined analogously. Our approach ensures self-consistency across the conditioning variables in the conditional extremes approach, since $\hat{\alpha}_{G,1} = 1$ if and only if $\hat{\alpha}_{G,2} = 1$; this issue is also discussed in [Liu and Tawn \(2014\)](#). A pictorial illustration of the estimation of η , $\lambda(\omega)$, $\tau_1(\delta)$ and α_1 is given in [Simpson and Tawn \(2022\)](#).

4.3 Estimation of the conditional scaling parameter β_i

As discussed in Section 2.3, the parameter β_i , $i = 1, 2$, in the conditional extremes framework is also linked to the asymptotic shape of a scaled sample cloud. However, the required feature of the set G is very subtle, and reliably estimating β_i using our estimate \hat{G} is not really feasible. Instead, we estimate β_i with α_i fixed to its estimated value, $\hat{\alpha}_{G,i}$ of expression (18). Illustrating this for β_1 , limit (5) is taken as an equality for some finite, but large, threshold u . Then, for $X_1 = x > u$ and with $a_1(x) = \hat{\alpha}_{G,1}x$ and $b_1(x) = x^{\beta_1}$, this implies that

$$X_2|(X_1 = x) = \hat{\alpha}_{G,1}x + x^{\beta_1}Z, \quad x > u,$$

where Z is a non-degenerate random variable that is independent of X_1 . It is common to take $Z \sim \mathcal{N}(\mu, \sigma^2)$ as a working assumption, for $\mu \in \mathbb{R}$, $\sigma > 0$ (see, e.g., [Keef et al. \(2013\)](#)), although other approaches have been considered (e.g., [Lugrin et al. \(2016\)](#)), which implies that

$$X_2|(X_1 = x) \sim \mathcal{N} \left\{ (\hat{\alpha}_{G,1}x + x^{\beta_1}\mu), (x^{\beta_1}\sigma)^2 \right\}, \quad x > u. \quad (19)$$

From this, it is straightforward to obtain maximum likelihood estimates for the parameters, with $\hat{\beta}_{G,1}$ denoting the corresponding estimate for β_1 .

4.4 Existing estimation techniques

We now present some existing estimators for the extremal dependence properties of Section 2.2. [Ledford and Tawn \(1996\)](#) estimate η using a maximum-likelihood based approach, which results in a Hill-type estimator ([Hill, 1975](#)), but on exponential margins. Setting $M = \min(X_1, X_2)$, and assuming we have $n_{u,H}$ observations of M above some high threshold u_H , denoted $m_1^*, \dots, m_{n_{u,H}}^*$, this estimator is

$$\tilde{\eta}_H = \frac{1}{n_{u,H}} \sum_{i=1}^{n_{u,H}} (m_i^* - u_H). \quad (20)$$

Alternative estimation procedures for η include the non-parametric approaches of [Peng \(1999\)](#) and [Draisma et al. \(2004\)](#). These aim to avoid inconsistencies that arise in carrying out estimation using different marginal distributions, which can result in issues when quantifying uncertainty. Suppose we

have n pairs of observations $(x_{1,1}, x_{1,2}), \dots, (x_{n,1}, x_{n,2})$, and denote by $x_i^{(j)}$ the j th largest value of component $i \in \{1, 2\}$, i.e., $x_i^{(n)} \leq x_i^{(n-1)} \leq \dots \leq x_i^{(1)}$. In both approaches, for each $j \in \{1, \dots, n\}$, the first step is to define the quantity $s_n(j) = \sum_{\ell=1}^n \mathbf{1}\{x_{\ell,1} \geq x_1^{(j)}, x_{\ell,2} \geq x_2^{(j)}\}$, with $\mathbf{1}(E)$ the indicator of event E . The estimators $\tilde{\eta}_P$ of Peng (1999) and $\tilde{\eta}_D$ of Draisma et al. (2004) are

$$\tilde{\eta}_P = \frac{\log 2}{\log \{s_n(2c)\} - \log \{s_n(c)\}}, \quad \tilde{\eta}_D = \frac{\sum_{j=1}^c s_n(j)}{cs_n(c) - \sum_{j=1}^c s_n(j)},$$

where c relates to the number of exceedances above a high threshold. Further details on these estimators can be found in Beirlant et al. (2004). Although $\eta \in (0, 1]$, all three of these estimators can result in values greater than one. Therefore, the truncated estimators $\hat{\eta}_H = \min(\tilde{\eta}_H, 1)$, $\hat{\eta}_P = \min(\tilde{\eta}_P, 1)$ and $\hat{\eta}_D = \min(\tilde{\eta}_D, 1)$ are preferable. The estimator we propose in Section 4.2 guarantees that $\hat{\eta}_G \in (0, 1]$ due to the scaling procedure proposed in Section 3.2.

Wadsworth and Tawn (2013) also discuss the use of a Hill-type estimator for $\lambda(\omega)$, analogous to $\hat{\eta}_H$, but taking $M_\omega = \min\{X_1/\omega, X_2/(1-\omega)\}$, for $\omega \in [0, 1]$. If we have $n_{u,\omega}$ observations of M_ω above a high threshold u_ω , denoted $m_{\omega,1}^*, \dots, m_{\omega,n_{u,\omega}}^*$, the estimator is given by

$$\tilde{\lambda}_H(\omega) = \left\{ \frac{1}{n_{u,\omega}} \sum_{i=1}^{n_{u,\omega}} (m_{\omega,i}^* - u_\omega) \right\}^{-1},$$

i.e., the reciprocal of the estimated mean excess of M_ω above the threshold u_ω . Again, the truncated estimator $\hat{\lambda}_H(\omega) = \min(\tilde{\lambda}_H(\omega), 1)$ is preferred. Similarly, Simpson et al. (2020) propose a Hill-type estimator for the coefficients $\tau_1(\delta)$, $\delta \in (0, 1]$. The idea is to slightly alter representation (4), and instead consider $\Pr(X_1 > x, X_2 \leq \delta X_1)$, for which estimation is simpler and Nolde and Wadsworth (2022) show also has the index of regular variation $\tau_1(\delta)$. Let $M_\delta = \{X_1 > 0 : X_2 \leq \delta X_1\}$. Suppose we have $n_\delta \leq n$ such observations of X_1 in our sample where $X_2 \leq \delta X_1$, and that $n_{u,\delta}$ of these, denoted $m_{\delta,1}^*, \dots, m_{\delta,n_{u,\delta}}^*$, are above some high threshold u_δ . Then,

$$\tilde{\tau}_{H,1}(\delta) = \frac{1}{n_{u,\delta}} \sum_{i=1}^{n_{u,\delta}} (m_{\delta,i}^* - u_\delta).$$

Again, we could have $\tilde{\tau}_{H,1}(\delta) > 1$ here, so we truncate to give $\hat{\tau}_{H,1}(\delta) = \min\{\tilde{\tau}_{H,1}(\delta), 1\}$.

5 Results - simulation study and data example

5.1 Simulation study

We demonstrate the performance of our proposed estimation procedure through a simulation study, providing a comparison to current estimators where these are available. We begin by considering estimation of the complete set G for the first three copulas from Figure 1, with $\rho, \gamma = 0.5$. For each copula, with exponential margins, we take a sample of size 10,000 and use the estimator \hat{G} of (15). This is repeated 100 times for each model, with the resulting estimates \hat{G} shown in Figure 4, alongside the true G . To obtain these results, we select the tuning parameters as stated in Section 3.3.

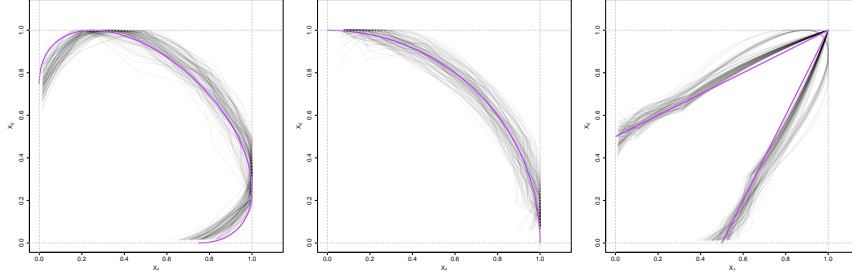


Figure 4: Estimates \hat{G} for the Gaussian (left), inverted logistic (centre) and logistic (right) models, with the corresponding ρ or γ parameters set to 0.5. The sample size in each case is $n = 10,000$ and 100 estimates are shown for each model (grey). The true sets G are shown in purple.

Spline degree	Gaussian	Inverted logistic	Logistic
1	39	37	78
2	48	19	3
3	13	44	19

Table 2: The number of times each spline degree is chosen for the estimated sets \hat{G} shown in Figure 4.

There is reasonable agreement between \hat{G} and G in Figure 4 for all three copulas. In the Gaussian and inverted logistic cases, the shapes of G are generally well represented by \hat{G} . For the logistic case, there are some estimates where the pointed shape of G has not been captured, but the estimates are reasonably successful overall. The degree of the spline chosen to model the log-scale parameter and threshold in the GPD plays an important role in determining the shape of \hat{G} ; in Table 2, we summarise the selected spline degrees over the 100 replicated data sets for each copula. Since G is smooth for both the Gaussian and inverted logistic copulas, we would expect to see the procedure favouring quadratic or cubic splines. For both these copulas, there is no overwhelming favourite in terms of the spline degrees chosen, but the non-linear options are selected around 60% of the time. On the other hand, the pointed shape of G for the logistic copula suggests that linear splines should be preferred here, with this being achieved in almost 80% of cases, and $(1, 1) \notin \hat{G}$ corresponding to the selection of quadratic or cubic splines.

As discussed in Section 4.2, once we have \hat{G} , we can use this to induce estimates of various extremal dependence properties. For estimating η , we compare our $\hat{\eta}_G$ given in (17), with the existing estimators $\hat{\eta}_H$, $\hat{\eta}_P$ and $\hat{\eta}_D$ described in Section 4.4. We fix the threshold u_H used in the estimator $\hat{\eta}_H$ to coincide with c for the estimators $\hat{\eta}_P$ and $\hat{\eta}_D$, such that all estimators use 500 data points. As with the tuning parameters in our approach, we have not optimised these choices, but have selected values that we found to work reasonably well across a range of examples. We take the set-up of our study as the same as for the results in Figure 4, but now take $\rho, \gamma \in \{0.25, 0.5, 0.75\}$; the η estimates are shown in Figure 5.

For the Gaussian copula, the existing approaches underestimate the true value of η , while our approach tends to overestimate by a similar magnitude, although our 95% confidence interval does contain the truth in each case and is generally the narrowest. For the inverted logistic copula, both $\hat{\eta}_G$ and $\hat{\eta}_H$, from (20),

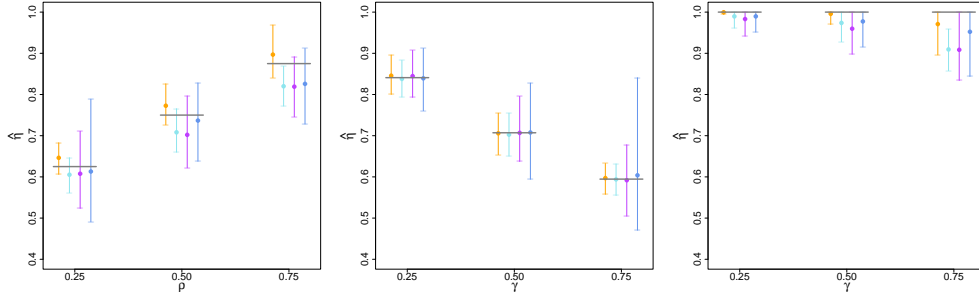


Figure 5: Estimates of η for data simulated from Gaussian (left), inverted logistic (centre) and logistic (right) copulas with their corresponding parameters taken as 0.25, 0.5 and 0.75. We show the mean estimates of η (circles) and 0.025 to 0.975 quantile range from 100 replicates for $\hat{\eta}_G$ (orange), $\hat{\eta}_H$ (light blue), $\hat{\eta}_P$ (purple), $\hat{\eta}_D$ (dark blue), each based on a data sample of 10,000. The true η values, summarised in Table 1, are shown in grey.

perform consistently well across the different values of γ ; all estimators appear to be unbiased but $\hat{\eta}_P$ and $\hat{\eta}_D$ suffer from increasing variability. The similarity of $\hat{\eta}_G$ and $\hat{\eta}_H$ is due to the fact that for this copula, step 2b of our scaling/truncation procedure is generally not required. Where $\hat{\eta}_G$ is particularly successful is in the logistic case, with asymptotic dependence and $\eta = 1$. Across all values of γ , we outperform the existing estimators, with clear success in Figure 5 for $\gamma \in \{0.25, 0.5\}$, where the dependence is stronger. For $\gamma = 0.75$, the picture is less clear, so we find the root mean square error for each of the estimators in this case; these are 0.048, 0.095, 0.103 and 0.069 for $\hat{\eta}_G$, $\hat{\eta}_H$, $\hat{\eta}_P$ and $\hat{\eta}_D$, respectively, confirming that $\hat{\eta}_G$ provides improvement over previous approaches. In terms of self-consistency for the logistic copula, while our approach satisfies the required property that $\eta \geq \max(\alpha_1, \alpha_2)$ in all cases, this is only true for 46%, 40% and 63% of the $\hat{\eta}_H$, $\hat{\eta}_P$ and $\hat{\eta}_D$ estimates in Figure 5, respectively, when compared to the maximum likelihood estimator for α_i , $i = 1, 2$ (results for which are given in Simpson and Tawn (2022)). The existing estimators are almost always self-consistent in our study for the Gaussian and inverted logistic copulas, where η is much larger than $\alpha_1 = \alpha_2$, but our approach still has the benefit that this coherence is guaranteed.

In Figure 6, we present estimates of $\tau_1(\delta)$, comparing our procedure to $\hat{\tau}_{H,1}(\delta)$, described in Section 4.4. Following Simpson et al. (2020), we fix the threshold u_δ used in the calculation of $\hat{\tau}_{H,1}(\delta)$ to the observed 0.85 quantile of the variable M_δ . Since we restrict \hat{G} to values within the range of observed angular values, there are some values of δ for which we cannot compute $\hat{\tau}_{G,1}(\delta)$. To ensure a fair comparison, we present the estimates $\hat{\tau}_{H,1}(\delta)$ over the same range of δ . In terms of bias, the two procedures are relatively similar, but there are two features to highlight in our estimates. First, only 18.6% of the $\hat{\tau}_{H,1}(\delta)$ estimates in Figure 6 (measured over 0.01 increments of δ) satisfy the required monotonicity property of $\tau_1(\delta)$, while our approach guarantees this aspect of self-consistency across different δ values in 100% of cases. Second, for small values of δ , $\hat{\tau}_{H,1}(\delta)$ has much greater variability than $\hat{\tau}_{G,1}(\delta)$ for all three copulas with $\rho, \gamma = 0.5$. This arises as $\hat{\tau}_{G,1}(\delta)$ ‘borrows’ more information from nearby values of δ than $\hat{\tau}_{H,1}(\delta)$, and therefore suffers less from the lack of data associated with estimates for small δ values.

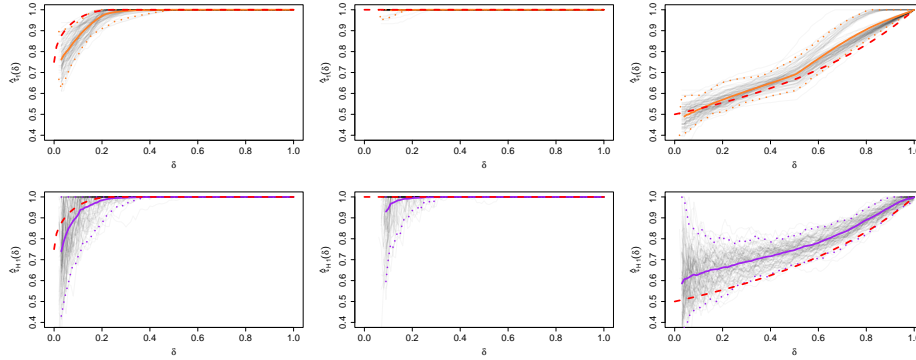


Figure 6: Estimates of $\tau_1(\delta)$, $\delta \in [0, 1]$, for data simulated from Gaussian (left), inverted logistic (centre) and logistic (right) models with their corresponding parameters set as 0.5. Each grey line represents an estimate obtained using $\hat{\tau}_{G,1}(\delta)$ (top) or $\hat{\tau}_{H,1}(\delta)$ (bottom) over 100 simulations. The solid and lower/upper dotted lines show the pointwise bootstrapped means and 0.025 and 0.975 quantiles, respectively, for $\hat{\tau}_{G,1}(\delta)$ (orange) and $\hat{\tau}_{H,1}(\delta)$ (purple). The true $\tau_1(\delta)$ values, summarised in Table 1, are shown in red.

Simpson and Tawn (2022) give further results for $\tau_1(\delta)$, using parameters $\rho, \gamma \in \{0.25, 0.75\}$ for the copulas used in Figure 6; with similar improvements in the logistic case with $\gamma = 0.25$. They also provide results for estimation of the features $\lambda(\omega)$, α_1 and β_1 . They find that $\hat{\lambda}_G(\omega)$ and $\hat{\lambda}_H(\omega)$ both provide successful estimates for the inverted logistic model across a range of dependence parameters γ , with $\hat{\lambda}_G(\omega)$ providing smoother estimates; our approach exhibits less bias than $\hat{\lambda}_H(\omega)$ in Gaussian cases; and we improve on the current approach in terms of variability for data from a logistic model. Our estimates of (α_1, β_1) are reasonably similar to those obtained from carrying out maximum likelihood estimation for both parameters α_1 and β_1 simultaneously, i.e., replacing $\hat{\alpha}_{G,1}$ in (19) with α_1 to be estimated.

5.2 Asymmetric logistic example

The three copulas we considered in Section 5.1 exhibit either asymptotic independence, or asymptotic dependence where both variables can only take their largest values simultaneously. We now demonstrate our approach for the asymmetric logistic model (Tawn, 1988), which can exhibit a mixture structure in its extremal dependence features, as discussed in Section 2.3.

We apply our estimation procedure to three samples of size 10,000 from the asymmetric logistic model with different values of θ_1 and θ_2 (which we take to be equal). The value of χ for this model is given in Appendix A. If $\theta_1 = \theta_2 = \theta$, we have $\chi = (2 - 2^\gamma)(1 - \theta)$, i.e., the strength of asymptotic dependence decreases as the value of θ increases. We fix the tuning parameters as in Section 5.1, and the resulting \hat{G} estimates are shown by the red dashed lines in Figure 7. This estimated boundary set is reasonably close to the truth for $\theta = 0.25$ and $\theta = 0.5$, where a respective 75% and 50% of the extremal mass is associated with both variables being simultaneously large (Simpson et al., 2020). When $\theta = 0.75$, so the proportion of mass associated with the simultaneously extreme variables is reduced to 25%, it becomes more difficult for \hat{G} to detect this feature. Results for additional simulations are given in Simpson and Tawn (2022).

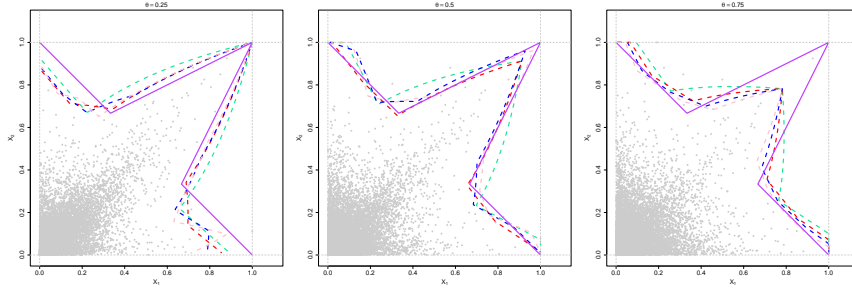


Figure 7: An example of our estimation procedure for the asymmetric logistic model with $\gamma = 0.5$ and $\theta \in \{0.25, 0.5, 0.75\}$. The true set G is demonstrated by the purple lines; the simulated data used to obtain the estimates of G are shown in grey; the dashed lines show our estimates of G for different numbers of knots in the spline functions ($\kappa = 5$: green; $\kappa = 7$: red; $\kappa = 9$: blue; $\kappa = 11$: pink).

We also carry out our estimation procedure using different numbers of knots κ in the spline functions of the GAMs, as here G is not smooth everywhere and increasing the number of knots may enable us to better capture this feature. Results with $\kappa \in \{5, 9, 11\}$ are shown in Figure 7. The results for $\kappa = 5$ are indeed slightly worse than for $\kappa \in \{7, 9, 11\}$, but otherwise our estimates of G are not particularly sensitive to this tuning parameter. An issue highlighted in Figure 7 is that our approach to scaling the boundary estimate onto $[0, 1]^2$ means we are unlikely to have our estimate of G intersecting each of the lines $x_1 = 1$ and $x_2 = 1$ in more than one region. As a result, it is difficult for our approach to detect extremal dependence mixture structures. We expand further on this point in our discussion in Section 6.2.

5.3 Application to sea wave height data

We now apply our approach to hindcast values of significant wave heights for locations in the North Sea. These are a subset of the data studied by [Wadsworth and Tawn \(2012\)](#) and, as in their paper, we consider only data from the winter months of December to February to limit issues with non-stationarity. We take data from four locations lying on a transect from the north-west to the south-east. The data set covers a period of 31 years with eight observations associated with each day in our months of interest, resulting in a total of 22,376 observations per location. Transformation (11) is applied to each variable to ensure the margins are on the required standard exponential scale.

Figure 8 shows \hat{G} at three pairs of locations with varying distances between them, with the tuning parameters as in Section 5.1. Uncertainty is presented by implementing the stationary bootstrap scheme of [Politis and Romano \(1994\)](#) over 100 iterations with the mean block-length set to 16 observations, i.e., two days. The most noticeable feature in these results is the weakening dependence in the significant wave height data as the distance between the locations increases, as is expected in environmental settings. In addition, the uncertainty in our estimates increases with the distance between the locations. While previous methods could have captured the weakening dependence for single parameter values, we can see this change over the whole shape of \hat{G} , highlighting the value added by our approach.

For the closest pair of locations, we estimate the coefficient of tail dependence as $\hat{\eta}_G = 0.997$ with a 95%

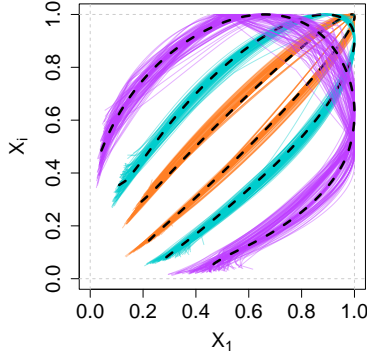


Figure 8: Estimates of G for significant wave heights at three pairs of locations in the North Sea (black dashed lines) with 100 bootstrapped estimates shown by the orange, turquoise and purple lines for locations at distances of approximately 40km, 130km, 300km, respectively. The variable X_1 represents the transformed and scaled significant wave heights at a location in the north-west of our study region; X_i ($i = 2, 3, 4$) corresponds to significant wave heights at the other locations.

confidence interval of $[0.994, 1.000]$; for comparison, we estimate $\hat{\eta}_H = 0.979$ $[0.961, 0.998]$. Our $\hat{\eta}_G$ suggests selecting a model that can capture asymptotic dependence would be most appropriate here, whereas using $\hat{\eta}_H$ the choice is more ambiguous due to a wider confidence interval that doesn't contain one. For the remaining two pairs of locations, the estimates are $\hat{\eta}_G = 0.974$ $[0.969, 0.983]$ and $\hat{\eta}_G = 0.897$ $[0.818, 0.924]$, respectively, with corresponding estimates $\hat{\eta}_H = 0.918$ $[0.887, 0.958]$ and $\hat{\eta}_H = 0.801$ $[0.739, 0.873]$. The $\hat{\eta}_G$ results both indicate that a model for asymptotic independence would be reasonable, although one may prefer the conservative approach of choosing an asymptotically dependent model for the former since the confidence interval is quite close to one. For all three pairs of locations, $\hat{\eta}_G > \hat{\eta}_H$, with narrower confidence intervals obtained for $\hat{\eta}_G$ than $\hat{\eta}_H$.

6 Discussion

6.1 Summary of the benefits of our approach

The aim of this paper was to develop a new inferential technique for bivariate extremes, allowing for self-consistent estimation for a range of extremal dependence features. This was motivated by recent theoretical developments by [Nolde \(2014\)](#) and [Nolde and Wadsworth \(2022\)](#), who showed that these features can all be linked to the asymptotic shape of a suitably-scaled sample cloud. We have demonstrated that our approach provides competitive results compared to currently available estimation techniques. As well as this, our method provides additional information not in existing measures, and comes with a number of desirable features that the existing methods do not; we highlight these here.

The main advantage of our approach over estimating each of the extremal dependence features separately, is that we achieve self-consistency in our estimates. One way to think about this is in terms of whether the parameter estimates indicate asymptotic dependence or asymptotic independence, since

separate estimation could lead to contradictions here. Consider the case of asymptotic dependence, where we know that we must have $\eta = 1$ and $\alpha_1 = \alpha_2 = 1$. In our inferential approach, we obtain $\hat{\eta}_G = 1$ exactly when our estimate of the set G contains the point $(1, 1)$, in which case we would also infer $\hat{\alpha}_{G,i} = 1$, $i = 1, 2$. The converse result is also true, meaning that we estimate $\hat{\eta}_G = 1$ if and only if $\hat{\alpha}_{G,1} = \hat{\alpha}_{G,2} = 1$. Neither of these possibilities are guaranteed when carrying out inference separately.

We mentioned in Section 2.2 that the set of measures $\{\eta, \tau_1(\delta), \tau_2(\delta)\}$ can be used to describe the extremal dependence structure of the variables. In particular, if X_1 can be large while X_2 is small, there must be some value of $\delta^* < 1$ such that $\tau_1(\delta^*) = 1$, and a similar result holds for $\tau_2(\delta)$. Moreover, if both variables can take their largest values simultaneously, then $\eta = 1$. Simpson et al. (2020) point out that

$$\max \{\eta, \tau_1(\delta) : \delta \in [0, 1)\} = \max \{\eta, \tau_2(\delta) : \delta \in [0, 1)\} = 1. \quad (21)$$

This constraint is not guaranteed by the estimators of η , $\tau_1(\delta)$ and $\tau_2(\delta)$ discussed in Section 4.4 (although one possible way to enforce this is discussed in Simpson (2019)). However, result (21) is naturally satisfied by our new estimation procedure, since the scaling/truncation steps ensure that \hat{G} intersects each of the lines $x_1 = 1$ and $x_2 = 1$ at least once.

Finally, the maximum likelihood estimation method for conditional extremes models, which we discussed in Section 4.2, involves placing a distributional assumption on Z . This may not be ideal in some cases, as there is the potential that mis-specifying the distribution could affect the resulting estimates of α_i and β_i . Our new approach has the benefit that we do not need to place a distributional assumption on Z for estimation of α_i , although we do for subsequent estimation of β_i . It may be possible that estimation of the set G could be improved to allow simultaneous estimation of α_i and β_i .

6.2 Potential issues and extensions

Throughout, we have assumed that our variables have standard exponential margins. A potential drawback of this, is that it restricts us to cases where there is independence or positive dependence between the variables, i.e., we cannot handle negatively dependent variables. For conditional extremes modelling, Keef et al. (2013) capture this feature by instead using Laplace margins; this possibility is also briefly discussed by Nolde and Wadsworth (2022). In practice, one could first test for negative dependence between the variables, and proceed with our approach only if it is not present in the data. It may also be possible to develop methodology similar to that presented here based on data initially transformed to Laplace margins, with the angular variable then on $[0, 2\pi)$.

We have discussed the possibility of having mixture structures in the extremal dependence, and there are different ways that this could arise. The framework of Simpson et al. (2020) identifies mixture structures where X_1 and X_2 can be simultaneously large but with the possibility of having each variable large while the other is of smaller order. Such a structure is indicated by $\eta = \max_{\delta < 1} \tau_1(\delta) = \max_{\delta < 1} \tau_2(\delta) = 1$; examples of sets G with this feature are given in the left plot of Figure 9, with $\delta^* = 0.2$, and the asymmetric logistic copula in Figure 1, with $\delta^* = 0$. The framework of Tendijck et al. (2022) also allows for a mixture structure in the extremal dependence but with the possibility of $\eta < 1$; this arises if G intersects

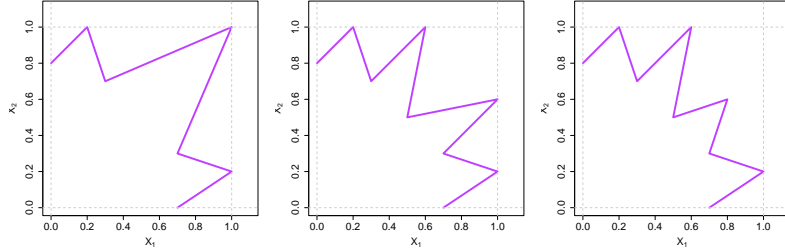


Figure 9: Examples of mixture structures in the set G .

at least one of the lines $x_1 = 1$ and $x_2 = 1$ at more than one separate location, as in the central panel of Figure 9. Our estimator \hat{G} was shown to be able to capture such non-convex shapes in the asymmetric logistic case, and therefore has the potential to be further exploited to test for mixture structures. To do this, the scaling/truncation step may need to be altered to ensure that \hat{G} intersects $x_1 = 1$ and $x_2 = 1$ an appropriate number of times, perhaps by first testing for convexity of the radial quantile estimates over w . A further interesting mixture possibility considered by [Tendijck et al. \(2022\)](#) is that of sub-asymptotic mixture components, as in the right panel of Figure 9, where we can see that for large X_1 , e.g., when $x_1 = 0.7$, there is a mixture of two possible ranges of X_2 values. In this case, the largest mixture component has a ‘point’ at $(0.8, 0.6)$ that does not reach the line $x_1 = 1$; this should also be taken into account if extending our approach as mentioned above.

The approach could be adapted to handle higher dimensional problems. An equivalent set G can be defined in higher dimensions; [Nolde \(2014\)](#) presents theoretical results on the coefficient of asymptotic independence in any dimension; [Nolde and Wadsworth \(2022\)](#) provide a result equivalent to (8) for calculating the indices of [Simpson et al. \(2020\)](#) in higher dimensions; and in the conditional approach of [Heffernan and Tawn \(2004\)](#), pairwise results can determine the relevant normalising functions. Our approach involves transforming to pseudo-polar coordinates, with only a one-dimensional angular component in the bivariate case. In a d -dimensional setting, the angular component would have dimension $d - 1$; this raises questions about how to select the angles used for local estimation to ensure reliability without a high computational cost. Moreover, the selection of the spline functions for \hat{G} comes with added complexity in higher dimensions, as different choices may be needed for different subsets of the variables. Future work that extends our approach to higher dimensions, should involve developing a strategy for selecting estimation points and spline functions in order to achieve scalable but reliable inference.

A further issue related to higher dimensional problems involves ensuring consistency across different dimensions. Suppose we have variables $\mathbf{X} = (X_i : i \in \mathcal{D})$, for $\mathcal{D} = \{1, \dots, d\}$. Using results on projections of sample clouds, [Nolde and Wadsworth \(2022\)](#) make links between gauge functions of lower dimensional subsets (for instance, variables indexed by $\mathcal{C} \subset \mathcal{D}$) to the gauge function associated with the full vector \mathbf{X} . This means that if our method were to be extended to higher dimensions, estimates of extremal dependence features for the variables $\mathbf{X}_{\mathcal{C}} = (X_i : i \in \mathcal{C})$ could be obtained by estimating the asymptotic boundary of the scaled sample cloud for any set of variables indexed by \mathcal{C}^* with $\mathcal{C} \subseteq \mathcal{C}^* \subseteq \mathcal{D}$. Ideally, we would like to ensure that consistent estimates are obtained from these different boundary estimates.

Code: Code to run the methods presented in this paper is available online in the GitHub repository <https://github.com/essimpson/self-consistent-inference>.

References

- Balkema, A. A. and Nolde, N. (2010). Asymptotic independence for unimodal densities. *Advances in Applied Probability*, 42(2):411–432.
- Beirlant, J., Goegebeur, Y., Segers, J., Teugels, J., and Vandewalle, B. (2004). Statistics of multivariate extremes. In Beirlant, J., Goegebeur, Y., Segers, J., and Teugels, J., editors, *Statistics of Extremes: Theory and Applications*, chapter 9, pages 297–368. John Wiley & Sons, Ltd, Chichester.
- Brozius, H. and de Haan, L. (1987). On limiting laws for the convex hull of a sample. *Journal of Applied Probability*, 24(4):852–862.
- Coles, S. G., Heffernan, J. E., and Tawn, J. A. (1999). Dependence measures for extreme value analyses. *Extremes*, 2(4):339–365.
- Coles, S. G. and Tawn, J. A. (1991). Modelling extreme multivariate events. *Journal of the Royal Statistical Society. Series B (Methodological)*, 53(2):377–392.
- Davis, R., Mulrow, E., and Resnick, S. I. (1987). The convex hull of a random sample in \mathbb{R}^2 . *Communications in Statistics. Stochastic Models*, 3(1):1–27.
- Davison, A. C. and Smith, R. L. (1990). Models for exceedances over high thresholds (with discussion). *Journal of the Royal Statistical Society: Series B (Methodological)*, 52(3):393–425.
- Draisma, G., Drees, H., Ferreira, A., and de Haan, L. (2004). Bivariate tail estimation: dependence in asymptotic independence. *Bernoulli*, 10(2):251–280.
- Eddy, W. F. and Gale, J. D. (1981). The convex hull of a spherically symmetric sample. *Advances in Applied Probability*, 13(4):751–763.
- Goix, N., Sabourin, A., and Cl emen on, S. (2017). Sparse representation of multivariate extremes with applications to anomaly detection. *Journal of Multivariate Analysis*, 161:12–31.
- Gumbel, E. J. (1960). Bivariate exponential distributions. *Journal of the American Statistical Association*, 55(292):698–707.
- Heffernan, J. E. and Tawn, J. A. (2004). A conditional approach for multivariate extreme values (with discussion). *Journal of the Royal Statistical Society: Series B (Methodological)*, 66(3):497–546.
- Hill, B. M. (1975). A simple general approach to inference about the tail of a distribution. *The Annals of Statistics*, 3(5):1163–1174.

- Keef, C., Papastathopoulos, I., and Tawn, J. A. (2013). Estimation of the conditional distribution of a multivariate variable given that one of its components is large: Additional constraints for the Heffernan and Tawn model. *Journal of Multivariate Analysis*, 115:396–404.
- Ledford, A. W. and Tawn, J. A. (1996). Statistics for near independence in multivariate extreme values. *Biometrika*, 83(1):169–187.
- Ledford, A. W. and Tawn, J. A. (1997). Modelling dependence within joint tail regions. *Journal of the Royal Statistical Society: Series B (Methodological)*, 59(2):475–499.
- Liu, Y. and Tawn, J. A. (2014). Self-consistent estimation of conditional multivariate extreme value distributions. *Journal of Multivariate Analysis*, 127:19–35.
- Lugrin, T., Davison, A. C., and Tawn, J. A. (2016). Bayesian uncertainty management in temporal dependence of extremes. *Extremes*, 19:491–515.
- Nolde, N. (2014). Geometric interpretation of the residual dependence coefficient. *Journal of Multivariate Analysis*, 123:85–95.
- Nolde, N. and Wadsworth, J. L. (2022). Linking representations for multivariate extremes via a limit set. *Advances in Applied Probability (to appear)*, <https://doi.org/10.1017/apr.2021.51>.
- Peng, L. (1999). Estimation of the coefficient of tail dependence in bivariate extremes. *Statistics & Probability Letters*, 43(4):399–409.
- Politis, D. N. and Romano, J. P. (1994). The stationary bootstrap. *Journal of the American Statistical Association*, 89(428):1303–1313.
- Resnick, S. I. (1987). *Extreme Values, Regular Variation, and Point Processes*. Springer, New York.
- Simpson, E. S. (2019). *Classifying and Exploiting Structure in Multivariate Extremes*. PhD thesis, Lancaster University.
- Simpson, E. S. and Tawn, J. A. (2022). Supplementary material for ‘Estimating the limiting shape of bivariate scaled sample clouds for self-consistent inference of extremal dependence properties’.
- Simpson, E. S., Wadsworth, J. L., and Tawn, J. A. (2020). Determining the dependence structure of multivariate extremes. *Biometrika*, 107(3):513–532.
- Simpson, E. S., Wadsworth, J. L., and Tawn, J. A. (2021). A geometric investigation into the tail dependence of vine copulas. *Journal of Multivariate Analysis*, 184:104736.
- Tawn, J. A. (1988). Bivariate extreme value theory: Models and estimation. *Biometrika*, 75(3):397–415.
- Tendijck, S., Eastoe, E., Tawn, J. A., Randell, D., and Jonathan, P. (2022). Modelling the extremes of bivariate mixture distributions with application to oceanographic data. *Journal of the American Statistical Association (to appear)*, <https://doi.org/10.1080/01621459.2021.1996379>.

- Wadsworth, J. L. and Tawn, J. A. (2012). Dependence modelling for spatial extremes. *Biometrika*, 99(2):253–272.
- Wadsworth, J. L. and Tawn, J. A. (2013). A new representation for multivariate tail probabilities. *Bernoulli*, 19(5B):2689–2714.
- Youngman, B. D. (2019). Generalized additive models for exceedances of high thresholds with an application to return level estimation for U.S. wind gusts. *Journal of the American Statistical Association*, 114(528):1865–1879.
- Youngman, B. D. (2020). *evgam: Generalised Additive Extreme Value Models*. R package version 0.1.4.
- Yu, K. and Moyeed, R. A. (2001). Bayesian quantile regression. *Statistics & Probability Letters*, 54:437–447.

A Details on the asymmetric logistic model

In Section 2.3, we discussed the gauge function and boundary set for a bivariate extreme value copula with an asymmetric logistic model, and provided simulation examples for this model in Section 5.2. We now provide more detail on the form of this model.

In exponential margins, the bivariate extreme value distribution function has the form

$$F(x_1, x_2) = \exp \left[-V \left\{ \frac{-1}{\log(1 - e^{-x_1})}, \frac{-1}{\log(1 - e^{-x_2})} \right\} \right]$$

for $x_1, x_2 \geq 0$ and an exponent measure $V(x, y)$ satisfying certain conditions. For the asymmetric logistic model,

$$V(x, y) = \frac{\theta_1}{x} + \frac{\theta_2}{y} + \left\{ \left(\frac{1 - \theta_1}{x} \right)^{1/\gamma} + \left(\frac{1 - \theta_2}{y} \right)^{1/\gamma} \right\}^\gamma,$$

with $x, y > 0$, $\gamma \in (0, 1]$ and $\theta_1, \theta_2 \in [0, 1]$. For this model, we have

$$\chi = 2 - \theta_1 - \theta_2 - \left\{ (1 - \theta_1)^{1/\gamma} + (1 - \theta_2)^{1/\gamma} \right\}^\gamma.$$

For a fixed $\gamma < 1$, the parameters (θ_1, θ_2) control the extremal dependence structure of the variables (X_1, X_2) and the strength of asymptotic dependence. If $\theta_1 > 0$, it is possible for X_1 to be large while X_2 is small, and an analogous result holds for $\theta_2 > 0$. If $\max(\theta_1, \theta_2) < 1$, then both variables can take their largest values simultaneously.

In the case where $\theta_1, \theta_2 \in (0, 1)$, the asymmetric logistic model can be thought of as a mixture of a logistic model with independence. Asymptotically, proportions $\theta_1/2, \theta_2/2$ and $1 - (\theta_1 + \theta_2)/2$ of the extremal mass are associated with the cases where X_1 is large while X_2 is small, X_2 is large while X_1 is small, and (X_1, X_2) are simultaneously large, respectively. The gauge function of this model does not depend on (θ_1, θ_2) , and takes the form (3).

Supplementary Material for ‘Estimating the limiting shape of bivariate scaled sample clouds for self-consistent inference of extremal dependence properties’

Emma S. Simpson¹ and Jonathan A. Tawn²

¹Department of Statistical Science, University College London, Gower Street, London, WC1E 6BT, U.K.

²Department of Mathematics and Statistics, Lancaster University, LA1 4YF, U.K.

Abstract

The aim of this Supplementary Material is to provide additional details for the paper ‘Estimating the limiting shape of bivariate scaled sample clouds for self-consistent inference of extremal dependence properties’. In Section **A**, we discuss the selection of tuning parameters for our limit set estimates \hat{G}^L and \hat{G} , while Section **B** provides an illustration of our scaling/truncation approach and how we obtain estimates of several bivariate extremal dependence features from \hat{G} . The remainder of the Supplementary Material provides additional simulation results for our approach: in Section **C**, we present estimates of \hat{G} to test sensitivity to the extrapolation quantile q ; in Section **D**, we give results on estimating $\tau_1(\delta)$ for additional copula dependence parameters; Section **E** covers estimation of $\lambda(\omega)$; Section **F** provides results on the (α_i, β_i) parameters of the conditional extremes approach; and Section **G** provides additional simulation results for the asymmetric logistic copula discussed in Section 5.2.

A Tuning parameter selection

Our proposed estimation procedure for the set G , presented in Section 3 of the main paper, involves the choice of several tuning parameters. For \hat{G}^L in Section 3.2, the first step is to choose the value of k and the angular values w_j^* , for $j \in J_k$. The discussion in Section 2.1 of the main paper highlighted that whether or not the point $(1, 1)$ belongs to the set G can play a crucial role in distinguishing between asymptotic dependence and asymptotic independence. As a result, the value of G at $w = 1/2$ is of importance, so $1/2$ should be taken to be one of the estimation angles w_j^* . We only take w_j^* values within the range of observed angles, i.e., setting $w^m = \min_{i=1, \dots, n} w_i$ and $w^M = \max_{i=1, \dots, n} w_i$, we have $w_j^* \in [w^m, w^M]$ for all $j \in J_k$. Natural options for choosing the w_j^* values include splitting the interval $[w^m, w^M]$ into equal segments or using empirical quantiles of $\{w_1, \dots, w_n\}$. The former has the drawback that several w_j^* values could be selected without any nearby values in $\{w_1, \dots, w_n\}$. In such cases, the neighbourhood in (14) would need to be relatively large to allow for inference, but this would come at the cost of obtaining reliable estimates of $r_q(w)$, as that may change considerably over this range of w . We therefore prefer the latter approach, with w_j^* as the $(j-1)/(k-1)$ th empirical quantile of $\{w_1, \dots, w_n\}$, for $j = 1, \dots, k-1$, and $w_k^* = 1/2$. We take k to be odd so that if the angular distribution is symmetric, we can have an

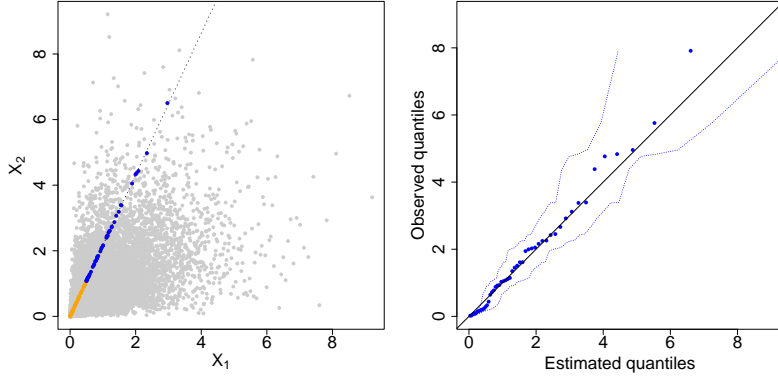


Figure A: Left: a sample of size 10,000 from an inverted logistic distribution with $\gamma = 0.5$ (grey) and an example of a set $\mathcal{R}_{w_j^*}$, with $|\mathcal{R}_{w_j^*}| = m = 100$ (orange: points in $\mathcal{R}_{w_j^*}$ below the empirical 0.5 quantile; blue: points in $\mathcal{R}_{w_j^*}$ above the empirical 0.5 quantile). Right: QQ-plot for the fitted GPD model for exceedances of $\mathcal{R}_{w_j^*}$ above the 0.5 quantile. The blue dashed lines represent approximate 95% confidence intervals for the pointwise empirical quantiles.

equal number of w_j^* values either side of $1/2$. Our studies suggest that the choice of k is not particularly crucial to the performance of the estimator, and we set $k = 199$ as a default.

Next consider the sizes of each radial neighbourhood $\epsilon_{w_j^*}$ ($j \in J_k$). We allow these to depend on the angle w_j^* , in order to control the size of each set $\mathcal{R}_{w_j^*}$. In particular, we fix each $\epsilon_{w_j^*}$ such that $|\mathcal{R}_{w_j^*}| = m$, for some choice of m . That is, $\mathcal{R}_{w_j^*}$ corresponds to the radial values of the m nearest angular neighbours of w_j^* . The GPD threshold $u_{w_j^*}$, or equivalently the value $q_u \in [0, q]$, also needs selecting. Figure A demonstrates an example of a single set $\mathcal{R}_{w_j^*}$ for the same data as in Figure 3. The QQ-plot in Figure A (right) suggests that taking $u_{w_j^*}$ as the empirical median of $\mathcal{R}_{w_j^*}$ (i.e., $q_u = 0.5$) is a reasonable choice, and we have observed the same behaviour over a range of different examples during our investigations. For simplicity, we therefore fix $q_u = 0.5$ in the paper. The final tuning parameter to select for the local approach is the value of q in (13). We have found values of q between 0.9 and 0.9999 to work well in practice, and take $q = 0.999$ subsequently. Sensitivity to this parameter is investigated in Section C, where the method appears robust to a reasonable range of choices of q .

When using the GAM framework to produce the smoothed estimates proposed in Section 3.3 of the main paper, we must select the number of knots (κ) and degree of the corresponding spline functions. For the reasons we discussed earlier, $w = 1/2$ is taken as one of the knots, which also suggests that an odd value of κ is reasonable. In practice, we suggest spacing the κ interior spline knots evenly throughout $[w^m, w^M]$, then adjusting the central one to be exactly $1/2$. Any required exterior knots are fixed at 0 and 1. We have found $\kappa = 7$ to be a reasonable choice in practice, illustrating the limited sensitivity to this tuning parameter in Section 5.2 of the main paper.

B Illustrations of our scaling/truncation and parameter estimation approaches

The scaling/truncation approach discussed in Section 3.2 of the main paper is demonstrated in Figure B. This allows for estimation of a finite set of points belonging to the set $G \subset [0, 1]^2$, with our final estimate given by $\hat{G}^L = \{(\hat{x}_{1,j}^G, \hat{x}_{2,j}^G) : j \in J_k\}$. In Figure C, we provide an illustration of our estimation procedure for η , s_ω (for $\lambda(\omega)$), $\tau_1(\delta)$ and α_1 . This accompanies the discussion in Section 4.2 of the main paper.

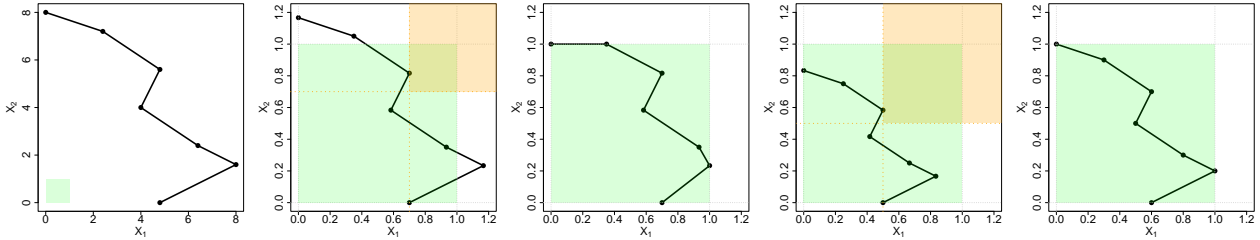


Figure B: An illustration of our scaling approach. From left to right, the first plot shows an example set of pre-scaled points $(\tilde{x}_{1,j}, \tilde{x}_{2,j})$, $j \in J_k$ (black dots), with $k = 7$ for illustrative purposes. The second plot demonstrates step 1 with $\hat{\eta}_H = 0.7$ including the set $[0.7, \infty]^2$ (orange region) and \hat{G}_η^L (black points) and the third plot shows the corresponding final set \hat{G}^L with points outside $[0, 1]^2$ transformed onto the boundary (step 2a). The fourth plot is equivalent to the second but with $\hat{\eta}_H = 0.5$, and the final plot shows the corresponding final set \hat{G}^L with the final transformation ensuring intersection with $x_1 = 1$ and $x_2 = 1$ (step 2b). The green region in each plot shows the set $[0, 1]^2$.

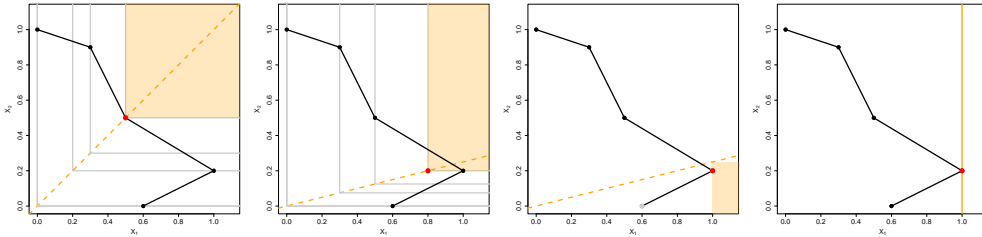


Figure C: A demonstration of how to obtain estimates of η , $s_{0.8}$ (for subsequent estimation of $\lambda(0.8)$), $\tau_1(0.25)$ and α_1 from the estimate of G . Here, \hat{G} uses $k = 5$ for illustrative purposes, but in practice k should be much larger. The black points in each plot demonstrate an estimated set \hat{G} . Left: the boundaries of the candidate sets $[s_j^*, \infty]^2$ for each point in \hat{G} (grey); the set $[\hat{\eta}_G, \infty]^2$ (orange region); and the point $(\hat{\eta}_G, \hat{\eta}_G)$ (red) which satisfies $x_1 = x_2$ (orange dashed line). Left-centre: the line $x_2 = \frac{1-0.8}{0.8}x_1 = 0.25x_1$ (orange dashed line); the boundaries of the candidate sets $[s_{0.8,j}^*, \infty] \times [0.25s_{0.8,j}^*, \infty]$ for each point in \hat{G} (grey); the set $[\hat{s}_{0.8}, \infty] \times [0.25\hat{s}_{0.8}, \infty]$ (orange region); the point of intersection of the orange region with \hat{G} (red). Right-centre: the line $x_2 = 0.25x_1$ (orange dashed line); the set $(\tau_1(0.25), \infty] \times [0, 0.25\tau_1(0.25)]$ (orange region); the point of intersection of the orange region with \hat{G} (red) and the other candidate for this intersection point (grey). Right: the line $x_1 = 1$ (orange) and its intersection with the set \hat{G} (red).

C Sensitivity to q

Our method involves the selection of several tuning parameters. Intuitively one of the most important is the value of q , representing the quantile of interest for the radial distributions before scaling onto $[0, 1]^2$. For all simulations and applications presented in the paper, we set $q = 0.999$, but we now present estimates of the set G for alternative quantile choices. All other tuning parameters are fixed as in Section 5.1 of the main paper. As in Figure 4 of the paper, we present results for data sets of size 10,000 simulated from Gaussian, inverted logistic and logistic models, repeating each test 100 times. The results are shown in Figure D for $q = 0.99$ and $q = 0.9999$. Overall, there is very little disparity between the estimates with q set as 0.99, 0.999 or 0.9999, since differences in the $r_q(w)$ estimates are offset by the subsequent scaling/truncation steps. There is some evidence that the estimates for the logistic model deteriorate as we increase q , with the least desirable quadratic spline option being chosen on five occasions for $q = 0.9999$ compared to zero with $q = 0.99$, although the linear spline options are still chosen in approximately 80% of cases. Hence, the estimates are overall not particularly sensitive to the choice of q , suggesting setting $q = 0.999$ is a reasonable choice.

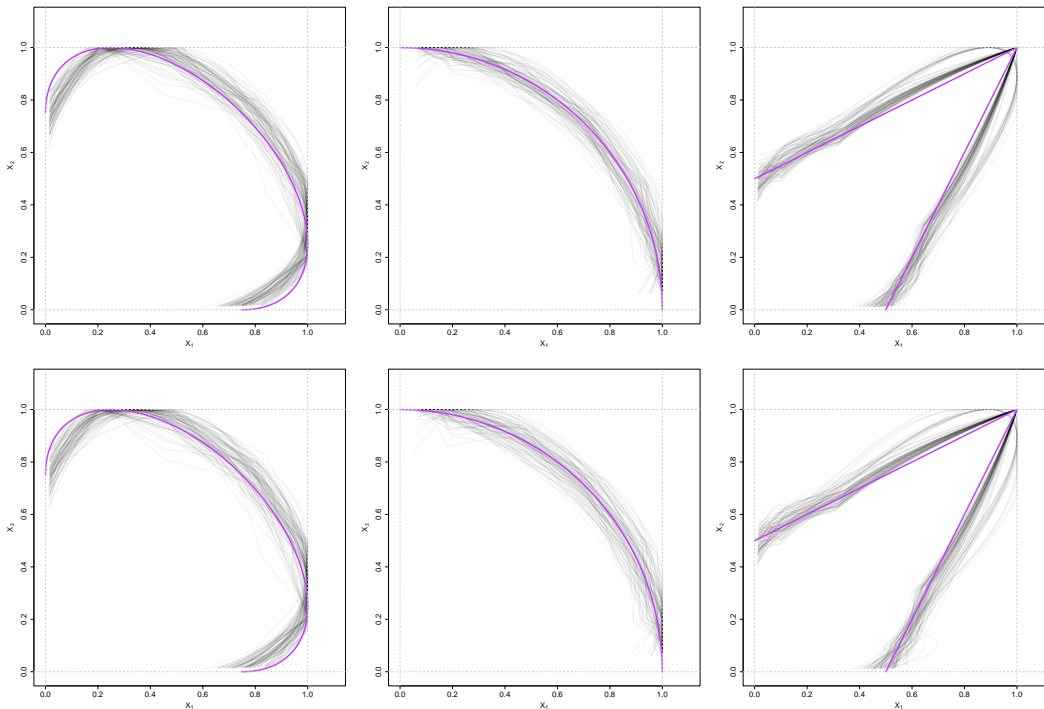


Figure D: Estimates of the sets G for the Gaussian (left), inverted logistic (centre) and logistic (right) copulas, with the corresponding ρ or γ parameters set to 0.5. The sample size in each case is $n = 10,000$ and 100 estimates are shown for each model (grey). The true sets G are shown in purple. The radial extrapolation quantile is set as $q = 0.99$ (top row) and $q = 0.9999$ (bottom row).

D Additional estimates of $\tau_1(\delta)$

In Figure 6 of the main paper, we presented results on estimation of the parameter $\tau_1(\delta)$ (Simpson et al., 2020) for Gaussian, inverted logistic and logistic models with parameters ρ or γ set to 0.5. In Figures E and F, respectively, we now present equivalent results for $\rho, \gamma = 0.25$ and $\rho, \gamma = 0.75$, comparing our new estimator to the Hill-type estimator $\hat{\tau}_{H,1}(\delta)$. We observe similar behaviour to that in the results of the paper. In particular, for smaller values of δ , our $\hat{\tau}_{G,1}(\delta)$ provides improvements in variance over the $\hat{\tau}_{H,1}(\delta)$ estimates. In terms of bias, our results are most successful in the inverted logistic cases and for smaller ρ and γ parameters. For $\rho = 0.75$, we tend to underestimate $\tau_1(\delta)$ for $\delta < 0.5$ in the Gaussian case, which is not a problem for the Hill-type estimator, while for $\gamma = 0.75$ both approaches yield overestimation in the logistic setting.

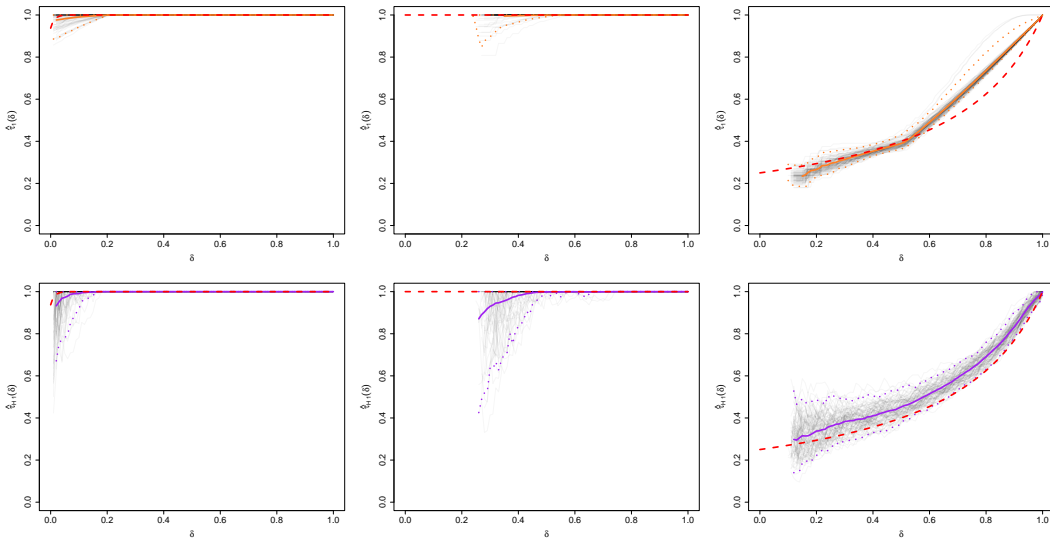


Figure E: Estimates of $\tau_1(\delta)$, $\delta \in [0, 1]$, for data simulated from Gaussian (left), inverted logistic (centre) and logistic (right) models with their corresponding parameters set as 0.25. Each grey line represents an estimate obtained using $\hat{\tau}_{G,1}(\delta)$ (top) or $\hat{\tau}_{H,1}(\delta)$ (bottom) over 100 simulations. The solid and lower/upper dotted lines show the pointwise bootstrapped means and 0.025 and 0.975 quantiles, respectively, for $\hat{\tau}_{G,1}(\delta)$ (orange) and $\hat{\tau}_{H,1}(\delta)$ (purple). The true $\tau_1(\delta)$ values are shown in red.

E Estimates of $\lambda(\omega)$

We now present results on the estimation of $\lambda(\omega)$. The simulation results presented in Figures G, H and I are analogous to those presented in Figures E, 6 (in the main paper) and F in the $\tau_1(\delta)$ case, respectively, i.e., for Gaussian, inverted logistic and logistic data with $\rho, \gamma \in \{0.25, 0.5, 0.75\}$. For the estimator $\hat{\lambda}_H(\omega)$, we set the threshold u_ω as the observed 0.95 quantile of the structure variable M_ω in each case. For the Gaussian examples, $\hat{\lambda}_H(\omega)$ has a tendency towards overestimation; this bias is significantly reduced by our proposed estimator. In the case of the inverted logistic data, the two approaches give comparable, unbiased

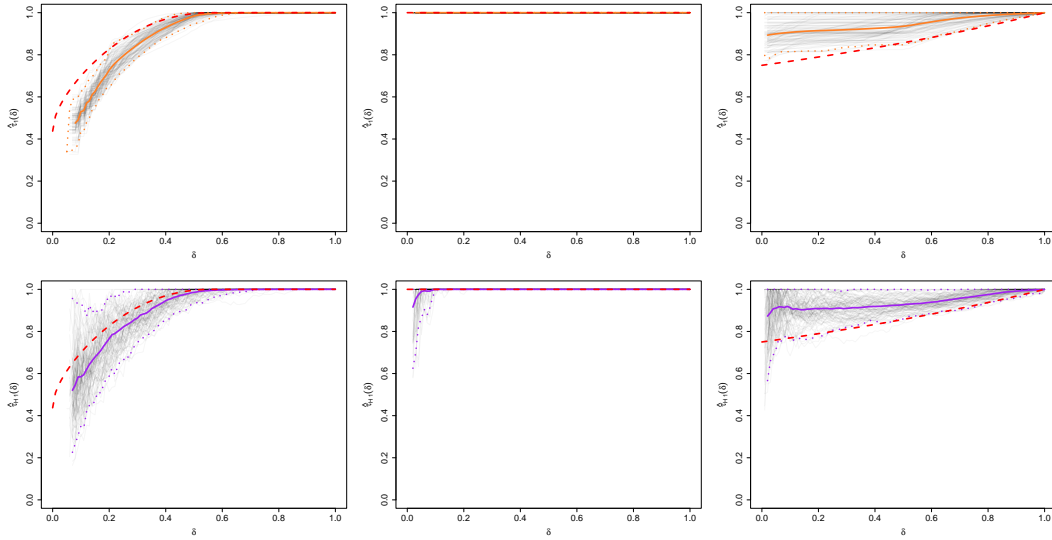


Figure F: Plots equivalent to Figure E, but with the copula parameters set to 0.75.

results with similar variability. Finally, for the logistic examples, with $\gamma = 0.25, 0.50$, our approach is particularly successful, giving almost perfect estimates of $\lambda(\omega)$ across the full range of $\omega \in [0, 1]$. For the logistic model with $\gamma = 0.75$, we also obtain strong results that are an improvement over the Hill-type estimator.

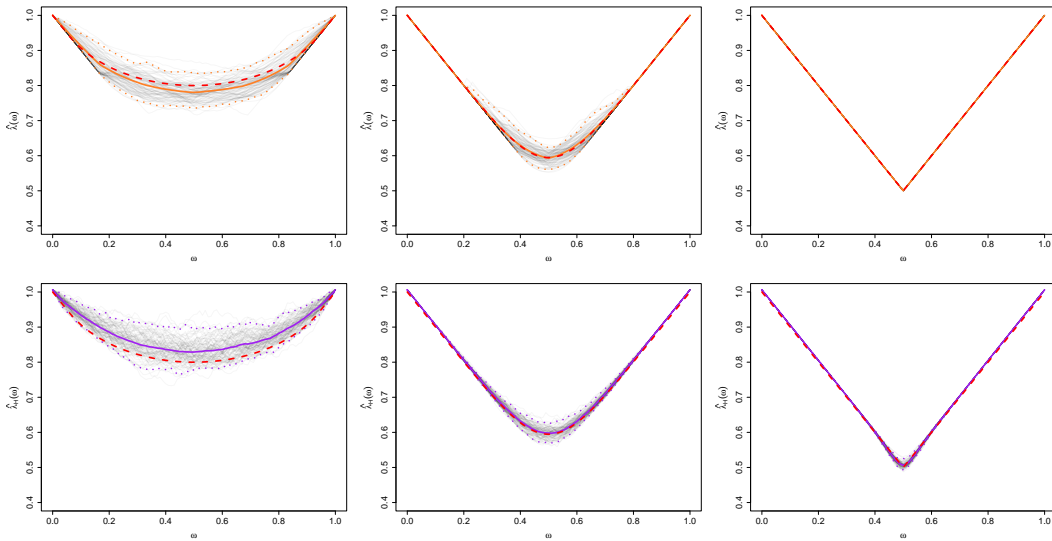


Figure G: Estimates of $\lambda(\omega)$, $\omega \in [0, 1]$, for data simulated from Gaussian (left), inverted logistic (centre) and logistic (right) models with their corresponding parameters set as 0.25. Each grey line represents an estimate obtained using $\hat{\lambda}_G(\omega)$ (top) or $\hat{\lambda}_H(\omega)$ (bottom) over 100 simulations. The solid and lower/upper dotted lines show the pointwise bootstrapped means and 0.025 and 0.975 quantiles, respectively, for $\hat{\lambda}_G(\omega)$ (orange) and $\hat{\lambda}_H(\omega)$ (purple). The true $\lambda(\omega)$ values are shown in red.

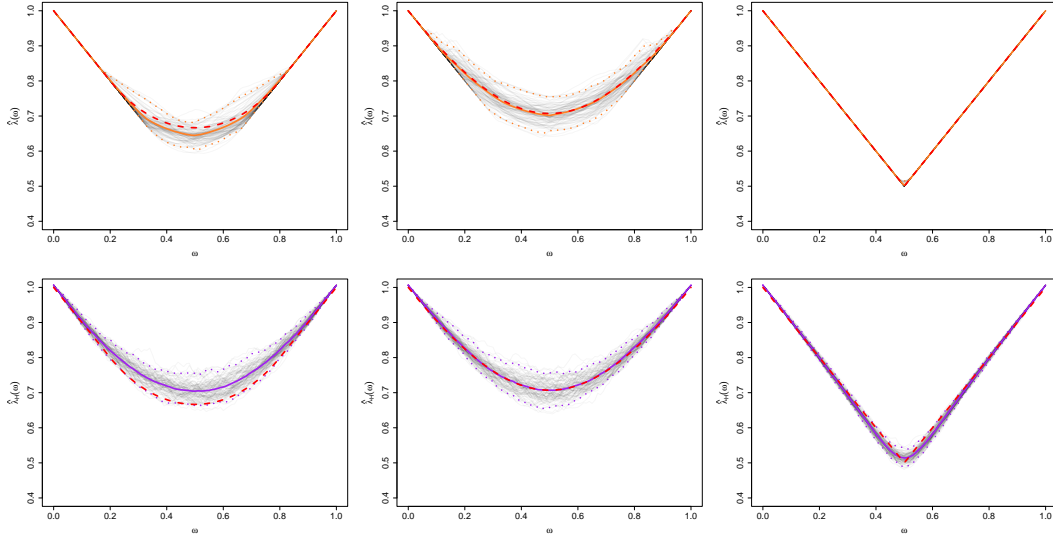


Figure H: Plots equivalent to Figure G, but with the copula parameters set to 0.5.

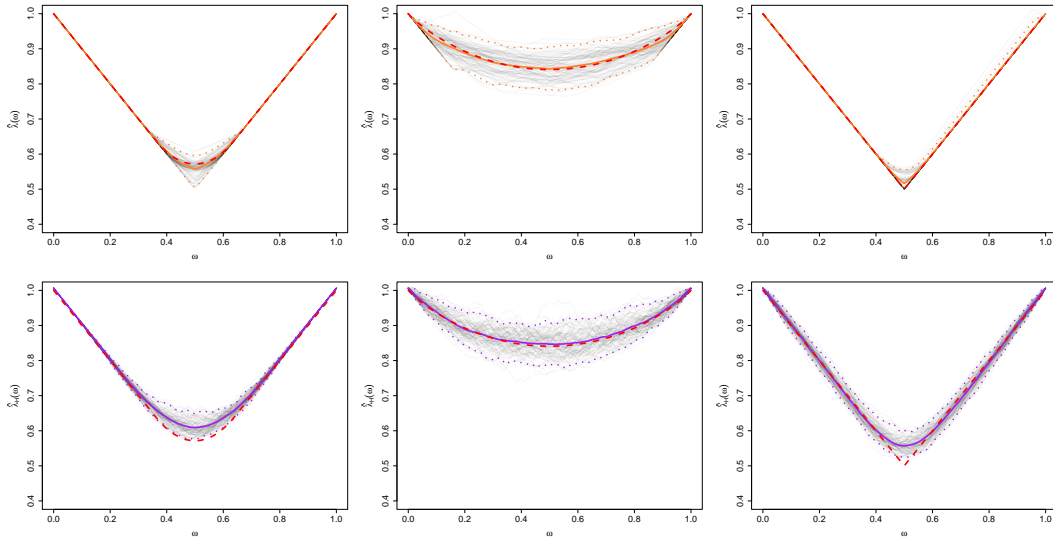


Figure I: Plots equivalent to Figure G, but with the copula parameters set to 0.75.

F Estimates of (α_1, β_1)

In Figure J, we present results on the estimation of α_1 and β_1 from the conditional extremes model of [Heffernan and Tawn \(2004\)](#). These are compared to results obtained using maximum likelihood estimators for model (19) for both parameters simultaneously. Our results are reasonably similar to those obtained using the maximum likelihood estimators, but slightly worse for inverted logistic data, although we do offer some improvement in the logistic case with $\gamma = 0.25, 0.5$. Most noticeably, neither approach is able to provide very successful estimation of the β_1 parameter, but this is known to be difficult to estimate.

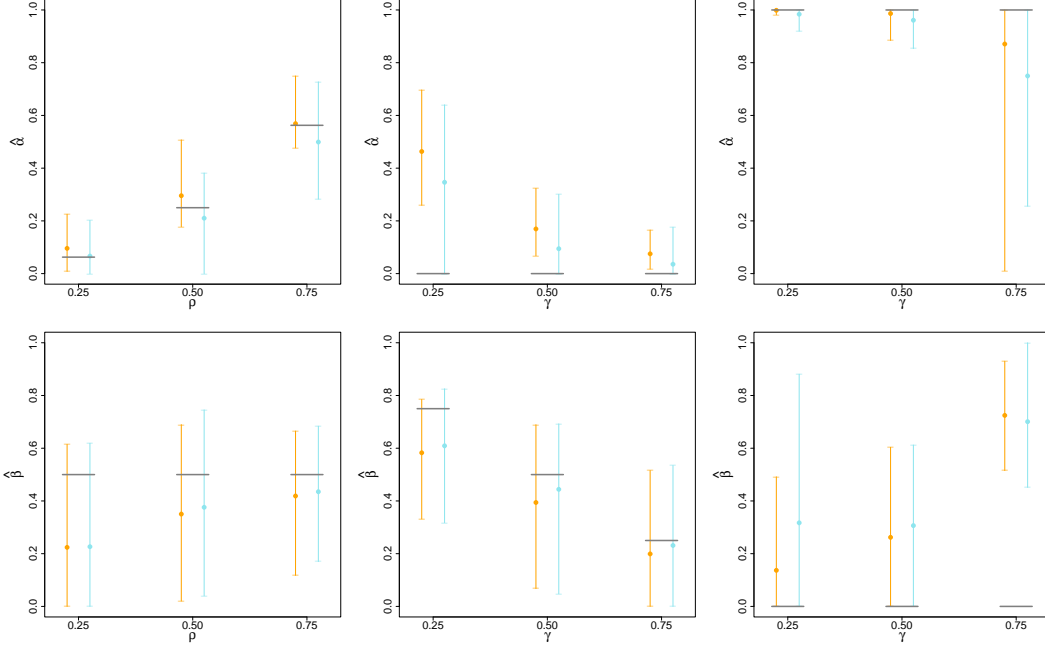


Figure J: Estimates of α_1 (top row) β_1 (bottom row) for data simulated from Gaussian (left), inverted logistic (centre) and logistic (right) models with their corresponding parameters taken as 0.25, 0.5 and 0.75. We show the mean estimates of β_1 (circles) and 0.025 to 0.975 quantile range over 100 simulations for $\hat{\beta}_{G,1}$ (orange) and maximum likelihood estimates of β_1 . The true β_1 values are shown in grey.

G Additional results for the asymmetric logistic model

In Section 5.2 of the main paper, we presented estimates \hat{G} for data simulated from an asymmetric logistic copula. One of the aims of Figure 7 there was to compare results over different numbers of knots κ used in the spline functions, focusing on a single data set. In Figure K, we present additional results over 100 repetitions for the default choice of $\kappa = 7$, with the remainder of the tuning parameters fixed as in Section 5.1. The estimates are similar to those given in Figure 7, with a similar amount of variability as in the Gaussian, inverted logistic and logistic cases of Section 5.1. In particular, we see that when $\theta = 0.75$, it remains difficult to completely capture the larger mixture component when X_1 is large for each sample replicate.

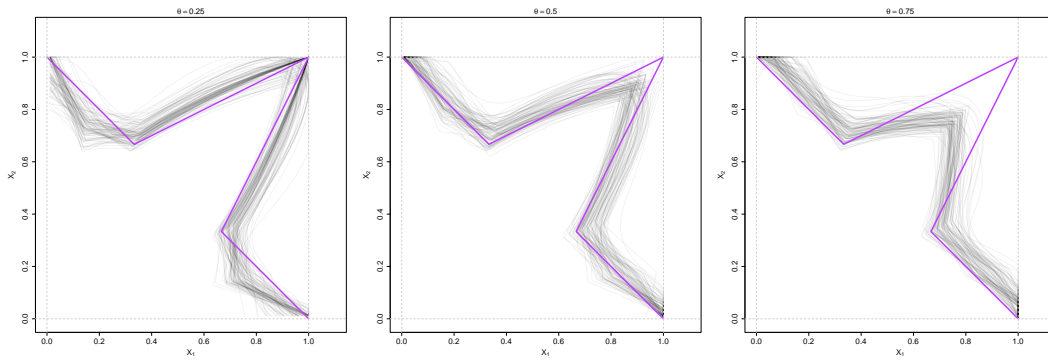


Figure K: Estimates \hat{G} for the asymmetric logistic copula with $\gamma = 0.5$ and $\theta \in \{0.25, 0.5, 0.75\}$ (left to right). The sample size in each case is $n = 10,000$ and 100 estimates are shown for each model (grey). The true sets G are shown in purple.